Conceptual design of a concrete multi-column floating platform supporting a 10 MW offshore wind turbine

By

Muhammad Sohail Hasan

A thesis presented to the

Graduate School of Urban Innovation

Yokohama National University

Yokohama, Japan

In partial fulfilment of the Requirements for the Degree of

Doctor of Philosophy in Engineering

Supervised by

Associate Prof. Chikako Fujiyama

September 2022

Yokohama National University, Japan

Graduate School of Urban Innovation

This thesis, written by Muhammad Sohail Hasan has been accepted by his advisor and thesis committee members. And, it is presented to Graduate School of Urban Innovation, Yokohama National University, Japan in partial fulfilment of the requirement for the degree of Doctor of Philosophy in Engineering.

Advisor	**Committee members**
Assoc. Prof. Chikako Fujiyama	Prof. Koichi Maekawa
	Prof. Akira Hosoda
	Prof. Hiroshi Katsuchi
	Prof. Motohiko Murai

Acknowledgment

Thanks to Allah Almighty for his unlimited kindness.

I wish to express my gratitude to my supervisor Dr. Chikako Fujiyama, for his guidance, encouragement at every stage and invaluable suggestions in this study. Her valuable advice and active interest in this topic were the source of my inspiration.

I am equally grateful to Dr. Rodolfo T. Gonçalves, Assistant Professor, Department of system Innovation, The University of Tokyo, Japan for his consistent guidance to the completion of my PhD research. Without his constant encouragement and guidance, this research project would not have been possible.

I am equally grateful to Dr. Edgard B. Malta, Director, Tecnhomar Engenharia Oceânica, Brazil for his consistent guidance and help in evaluating the hydrodynamic and aerodynamic behaviour of the proposed model.

I am also grateful to Dr. Koichi Maekawa, Professor, Civil Engineering Department, Yokohama National University, Japan, for guidelines in upgrading the research.

My deepest gratitude goes to Professor Akira Hosoda, whose comments during laboratory seminar helps to improve the research.

I am grateful to my colleagues and laboratory members especially Wichuda Munbua and Muhammad Talha Ghafoor for valuable discussion and help during research.

I am intensely grateful to the Government of Japan and Yokohama National University for awarding me the scholarship in the Department of Civil Engineering in PhD program. My appreciation also goes to all the current and the former laboratory members for their kind co-operation in every step of the author's present study and research.

A very special gratitude is offered to my wife Arsala Saeed, my both son Abdullah Hasan and Mahmood-ul-Hasan, my parents and siblings who are always constant sources of inspiration and support throughout my life.

Table of Content

Acknowledgment i

Table of Content ii

List of Tables vi

List of Figures vii

ABSTRACT 1

1 Introduction 2

1.1 Floating Wind Energy 2

1.1.1 Preamble 2

1.1.2 Offshore Wind Turbine Classifications 3

1.1.3 Wind turbine generator development 3

1.2 Research Motivation 3

1.3 Why Concrete is Important? 4

1.4 Challenges in installation of Concrete Floater 5

1.5 Objective 6

1.6 Outline of the Dissertation 6

2 Literature review 8

2.1 Overview of FOWT 8

2.1.1 Floating offshore wind concept 8

2.1.2 Background of Fatigue 9

2.2 Wind Turbine components 10

2.2.1 Nacelle 10

2.2.2 Blades 10

2.2.3 Rotor 10

2.2.4 Tower 11

2.2.5 Floating Platform 11

2.3 Major technologies in FOWT 11
2.3.1 Tension Leg Platform 11
2.3.2 Spar 11
2.3.3 Barge 12
2.3.4 Semi-submersible 12
2.4 Floating Offshore Wind Turbine Mechanics 13
2.4.1 Degree of freedom and coordinate system 13
2.5 Floating platform 14
2.5.1 Buoyancy and Gravity system 14
2.5.2 Hydrostatic stability 14
2.5.3 Equations of motions 15
2.5.4 Floating body Natural Frequency 16
2.6 Floating structure loads 16
2.6.1 Hydrostatic pressure 16
2.6.2 Diffraction and radiation 16
2.6.3 Morison's equations 17
3 A Case Study - FloatGen 18
3.1 First FOWT with RC Floater (FRANCE) 18
3.2 Finite element tool 18
3.2.1 Load pattern and connection details 19
3.3 Summary of chapter 22
4 Design of Panel Based Reinforced Concrete Floating Substructure for 10 MW Offshore Wind Turbine 23
4.1 Structural details of concrete floater based on geometric design 23
4.2 Structural design 25
4.2.1 Tower to Floater Connection Part 25
4.2.2 Slab Design 26

4.2.3 Wall Design and crack width criteria 27
4.2.4 Mooring Line to Floater Connection 29
4.3 Summary of chapter 30
5 Multi-Column Semi-Submersible Design Mission 31
5.1 Premises 31
5.1.1 Location 31
5.1.2 Depth 31
5.1.3 Reference Wind Turbine 31
5.1.4 Wave conditions 31
5.1.5 Wind conditions 32
5.2 Methodology 33
5.2.1 Parametric Model 34
5.3 Intact Stability 37
5.4 Summary of chapter 38
6 Dynamic Evaluation of Concrete Floater based on Parametric Model 39
6.1 Hydrodynamic Analysis 39
6.1.1 EdtoolsX 39
6.1.2 WAMIT 39
6.1.3 Added mass, restoring force, Inertial mass, Natural period 40
6.2 Response Amplitude Operators (RAOs) 41
6.2.1 Surge 41
6.2.2 Heave 42
6.2.3 Pitch 43
6.3 Spectral analyses 43
6.4 Aerodynamic Analysis 46
6.5 Mooring Tension 48
6.6 Summary of chapter 50

7 Model Test 52
7.1 Experimental setup 52
7.1.1 Scaled model 52
7.1.2 Wave conditions 54
7.1.3 Model test conditions 54
7.2 Data Analysis 55
7.3 Comparison of Heave Plate behavior under Operational and Storm Conditions 58
7.3.1 Heave Comparison 58
7.3.2 Pitch Comparison 59
7.3.3 Surge Comparison 60
7.4 Summary of chapter 61
8 Conclusions 62
8.1 Summary of the Chapters 62
8.2 Conclusions 62
8.3 Future Recommendations 63
9 References 64

List of Tables

Table 3-1Case study parametric models.....20
Table 4-1 Structural details of concrete floater 23
Table 4-2 Geometrical properties of RC floater.....24
Table 5-1: Wind Turbine Generator Properties.....32
Table 5-2 Wave Conditions.....32
Table 5-3 Wind Conditions 33
Table 5-4 Main dimension and variables considered in the parametric model studies 37
Table 6-1 Added mass, restoring force, Inertial mass, Natural period.....40
Table 6-2 Significant motion response results of the spectral analysis.....46
Table 6-3 Coupled dynamics results of OpenFAST analysis.....47
Table 6-4 Main properties of the proposed concrete FOWT.....48
Table 7-1 Selection of the case for Model test 52
Table 7-2 Main dimension and variables for the case used in model test.....53
Table 7-3 Irregular wave conditions in full scale.....54
Table 7-4 Regular wave conditions in full scale 55

List of Figures

Figure 1-1 Typical floating platform used in oil and gas industry [10] 2
Figure 1-2 Wind Turbine generator capacity and sizes (NREL) [11] 4
Figure 1-3 Floating runway Japan [19] 5
Figure 1-4 Offshore wind turbine platform corrosion [20] 6
Figure 2-1 Tension leg platform design [67] 11
Figure 2-2 Spar and Barge types of FOWT 12
Figure 2-3 Floating offshore wind turbine – Semi-submersible concept 13
Figure 2-4 Coordinate system 13
Figure 2-5 Floating bodies stability conditions 14
Figure 2-6 Metacentric height GM 15
Figure 3-1 Layout of Floatgen Ideol [15] 18
Figure 3-2 Concrete fatigue constitutive model used in COM3 [68] 19
Figure 3-3 Prestress load configuration 20
Figure 3-4 FE model and steel connectors of Ideol barge structure 20
Figure 3-5 Top view of the model and elements description 21
Figure 3-6 Steel Stresses in Mooring connection 21
Figure 3-7 Concrete stresses in the element adjacent to the steel connector 22
Figure 4-1 Proposed reinforced concrete floater 24
Figure 4-2 Optimum geometric comparison 25
Figure 4-3 Reinforcement under Tower base area 26
Figure 4-4 Anchorage at tower base 26
Figure 4-5 Slab reinforcement 27
Figure 4-6 Neutral axis and compression zone 29
Figure 4-7 Side wall design 29
Figure 4-8 Mooring connection for concrete floater 29
Figure 5-1 Wave Spectrums of Different Conditions on The Japanese Coast 33
Figure 5-2 An overview of research methodology 34
Figure 5-3 Variables of the design. Perspective view of a schematic 3d model. 34
Figure 5-4 Variables of the design. Top view of a schematic 3d model. 35
Figure 5-5 Schematic layout of the proposed floater 36
Figure 5-6 intact stability of the structure 37
Figure 6-1 EdtoolsX preface 39

Figure 6-2 Low order mesh considered in the WAMIT code 40
Figure 6-3 Heave added mass comparison 41
Figure 6-4 Comparison of Surge RAOs 42
Figure 6-5 Comparison of Heave RAOs 42
Figure 6-6 Comparison of Pitch RAOs 43
Figure 6-7 Wave spectrums of different conditions on the Japanese coast 44
Figure 6-8 Power spectrum of heave motion due to the operational condition 45
Figure 6-9 Power spectrum of pitch motion due to the operational condition 45
Figure 6-10 The correlation of hydrodynamics and aerodynamics 46
Figure 6-11 Comparison of heave RAOs of WAMIT and OpenFAST calculations 47
Figure 6-12 Comparison of pitch RAOs of WAMIT and OpenFAST calculations 47
Figure 6-13 Mooring line arrangement 49
Figure 6-14 Surge motions for Operational Sea states with rated wind speed 49
Figure 6-15 Toyota Arrows Bridge completed photo [90] 50
Figure 7-1 Full scale model dimensions used in the experiment 53
Figure 7-2 Model dimensions used in the experiment at the scale of 1:60 53
Figure 7-3 Towing tank dimensions 54
Figure 7-4 Types of models based on heave plates orientation 54
Figure 7-5 Wave Signal and Spectral Response of the Floater 55
Figure 7-6 Motion Signal and Spectral Response of the Floater 56
Figure 7-7 Wave Spectrums of Different Conditions on The Japanese Coast 56
Figure 7-8 Comparison of RAOs between Experiment and Analysis for Surge 57
Figure 7-9 Comparison of RAOs between Experiment and Analysis for Heave 57
Figure 7-10 Comparison of RAOs between Experiment and Analysis for Pitch 58
Figure 7-11 RAOs Heave Comparison for Operational conditions 58
Figure 7-12 RAOs Heave Comparison for Storm conditions 59
Figure 7-13 RAOs Pitch Comparison for Operational Conditions 59
Figure 7-14 RAOs Pitch Comparison for Storm Conditions 60
Figure 7-15 RAOs Surge Comparison for Operational Conditions 60
Figure 7-16 RAOs Surge Comparison for Storm Conditions 60

ABSTRACT

This thesis aims to design a concrete semi-submersible floating structure for a 10 MW wind turbine using precast panel-based concrete, i.e., a concrete floating offshore wind turbine (FOWT), using a parametric hull design methodology and optimization. The design was applied by considering different parameters, such as main floater dimensions, the thickness of the concrete panels, heave plate dimensions, the draft of the platform, and the thick concrete portion at the connecting part between the concrete floater and steel tower. Environmental conditions of waves and wind were selected from the Japanese coast to analyse the dynamic behaviour of the proposed concrete semi-submersible floater in waves and wind. A parametric hull design methodology was conducted based on some restrictions to generate feasible cases and to select the potential best solutions based on the restoring moment and natural periods of the floater. The curve was created by minimizing the nacelle's acceleration and the platform's structural mass. WAMIT and OpenFAST were used to calculate the hydrodynamic behaviour and the coupled analysis. A detailed comparison was presented for three cases; moreover, a best potential case was proposed as a final option. This thesis successfully illustrated the hydrostatic, hydrodynamic and aerodynamic behaviour to confirm the feasibility of this new concept of a concrete floater for 10 MW FOWT.

1 Introduction

1.1 Floating Wind Energy

1.1.1 Preamble

Floating offshore wind is relatively new field for power generation and have big capacity around the world. Lot of researchers are working on floating offshore wind platform as well as on wind turbines. Hywind is the world's first floating offshore wind form which was in operation by the end of 2017 [1].

In the report presented by International Renewable Energy Agency (IRENA), it is mentioned that world's 2/3rd greenhouse emission is due to energy production [2]. This is due to the mainly usage of fossil fuels for electricity production. The total electricity production by the end of 2020 was around 27000 TWh. Out of this electricity production 28% was from renewable resources i.e. solar power, hydropower, waves, bio power, geothermal power and wind power while 72% was from non-renewable resources [3].

Wind energy has a low environmental impact. Wind resources are also a clean, inexhaustible resource, besides economically feasible. In comparison to traditional resources, the environmental impacts are manageable [4]. In 2020, cumulative global installation of wind energy reached the capacity of 741.7 GW [5]. Wind energy production is divided into two major types: onshore wind energy and offshore wind energy. Previously, the major portion of energy production was from onshore. There are some disadvantages in onshore wind farms, such as the wind noise and the non-uniform wind speed [6]. There are two main reasons for increasing offshore wind energy production, the uniform wind speed and the available space for building offshore wind farms. Although the cost of offshore wind turbines is a bit high compared to other energy solutions, due to additional cost of cable laying on the seabed, for example, this issue can be countered by increasing the wind turbine size [7]. In turn, chances of uniform wind speed profile increased as we go deeper in the sea from the coast, which leads to smaller turbulence intensity [8]. Therefore, the life cycle of offshore wind turbine generator will be increased due to the smaller fatigue effect [9].

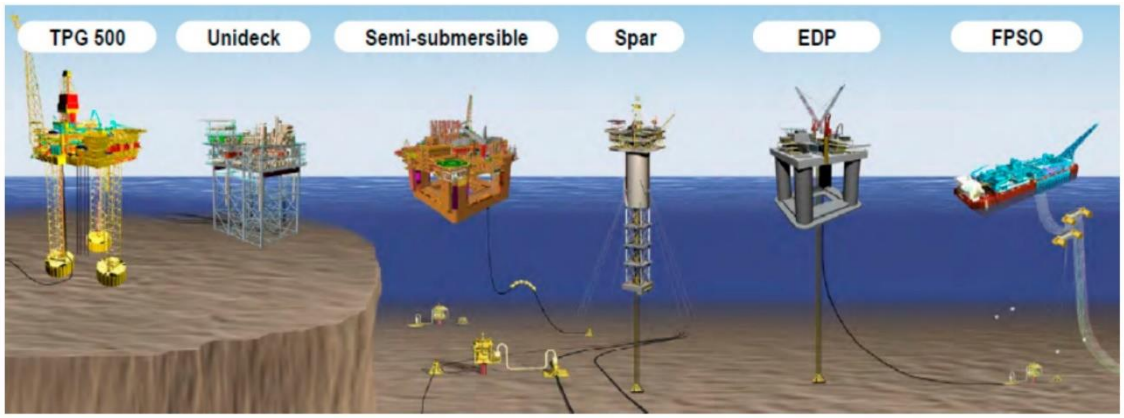

Figure 1-1 Typical floating platform used in oil and gas industry [10]

The concept of floating offshore wind turbine originated from oil and gas industry where floating platform is anchored with the seabed [10]. Many concepts for floating wind

platform like spar, semi-submersible and tension leg platform inspired from these technologies, few of them are shown in Figure 1-1.

The major problem in floating offshore wind turbine (FOWT) is the coupling of hydrodynamic loads and aerodynamic loads and coupling of wind turbine generator (WTG) with the supporting platform. This industry is still at an early stage and around 30 conceptual design are in development [10] and few are deployed around the world.

1.1.2 Offshore Wind Turbine Classifications

Based on the depth of water, offshore wind turbine foundations are divided into 3 main categories:

- Shallow water
- Transient water
- Deep water

Generally, shallow water offshore wind turbines are placed at the water depth of 5-30 m. The types of shallow water foundations are monopile foundation, gravity-based foundation and suction bucket type foundations.

Transient water offshore wind turbines are placed at the water depth of 30-60 m. These are named as guyed monopile, tripod tower, submerged jacket, full height jacket and enhanced gravity based or suction-based foundation.

The deep-water wind turbines are the floating offshore wind turbines and are divided into Tension leg platform, spar, barge and semi-submersible.

Currently, most of the floating offshore wind projects are located at the shallow or transient water depth. About 80% of offshore wind farms are fixed bottom foundations due to their comparatively easy design and fabrication. Moreover, the fixed bottom foundation supports energy production 2-5 MW whereas floating offshore wind turbine substructure may support energy production around 15 MW.

1.1.3 Wind turbine generator development

From the start of wind energy production till early 90s,the capacity of wind turbines was up to 300 KW with maximum hub height of 30 m. From early 90s to mid-2000, the wind turbine generator capacity increased to 2 MW with the hub height of 80 m as shown in Figure 1-2. From 2005 to onward wind turbine generator capacity increased and difficult to get the uniform wind speed on the onshore wind turbines. Now the pilot projects of 10 MW floating wind turbines are under fabrication / installation procedure [11].

1.2 Research Motivation

After 2011 nuclear accident in Fukushima, because of closure of power plants, Japan is facing high electricity shortage. This urges the government to get the electricity from renewable energy resources. Japan is enriched in offshore wind energy resources because of its long seashore availability but offshore wind energy production is very less which is only 62 MW by 2016 [12]. In 2016, 2 MW wind turbine was installed on the hybrid spar floating platform at Goto Island. Currently, Japanese government announced to obtain 40 GW of energy production from wind energy. Lot of researchers are working to propose the feasible and economical solutions to make this possible.

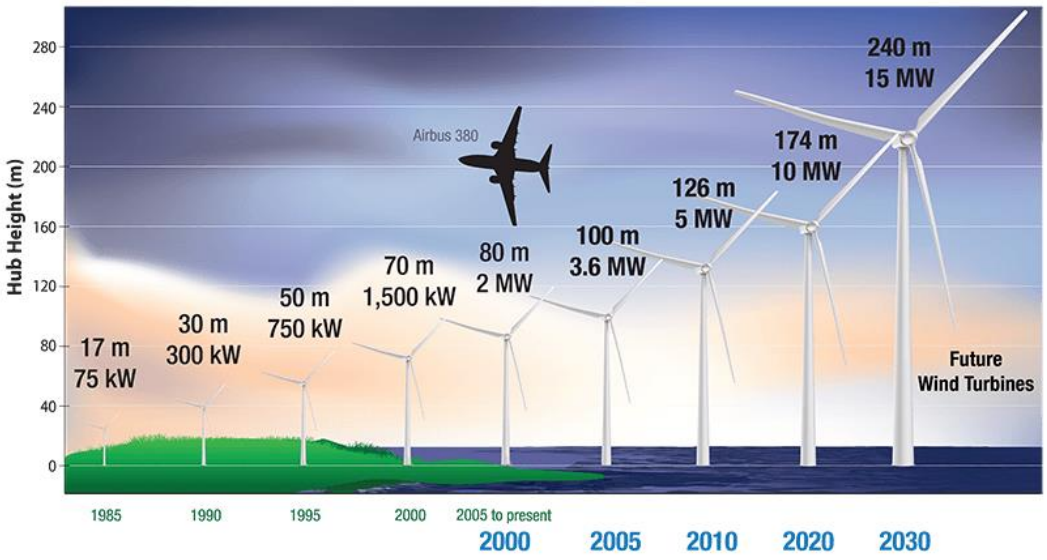

Figure 1-2 Wind Turbine generator capacity and sizes (NREL) [11]

There are some issues in the development of the floating offshore wind industry, among which are the limits in the fabrication processes, installation, and higher transportation costs. One of the options to decrease the costs may be to improve the wind turbine generator capacity, which was previously 5 MW, to achieve larger sizes for the initial developments of FOWT. As an example solution, there is a large capacity of 10 MW reference wind turbine improved the 5 MW proposed by the National Renewable Energy Laboratory (NREL) in 2013. When the wind turbine generator (WTG) capacity was increased, a higher capacity floating structure was needed with higher stability and better dynamic response to waves and wind. There are two main crucial parts in a FOWT: the first is the rotor-nacelle-assembly (RNA), and the second is the floating structure. The RNA does not usually depend on the location of the FOWT operation; however, the support structures for the wind turbine can be customized and optimized in terms of motion performance and operational time window for the specific site location.

The other challenge is until now few substructures for floating wind turbine for 10 MW or higher has been proposed. Out of these, only OO star wind floater has been successfully proposed based on concrete material and this will be constructed at the end of 2022. As a result, the decision was made to do research for checking the hydrodynamic, aerodynamic behaviour and coupling of wind turbine to the concrete floating substructure for 10 MW wind turbine.

1.3 Why Concrete is Important?

Concrete has merits when we compare it to the steel structures in floating offshore wind turbine. For steel mills, it takes time to start or stop the operation, so the price variation is common. As mentioned in the report by London metal exchange database [13], from 2008 to 2012, the price variation was in between 250$ to 1250$. On the other hand, cement cost in France was stable and price variation was within +/-3% [14].

Based on the above price, the cost for 6 MW concrete floater was approximately two times cheaper than steel floater of the same size [15].

For the construction of steel floaters, shipyard technique is required, and shipyards are not available all the time near the sites. While concrete structures can be built as a precast-prestressed panels in a factory or factory unit can be built at site if more number of concrete floaters are required [15].

Moreover, construction of steel floaters needs expertise or highly skilled labour as compared to concrete structures. As concrete construction is common everywhere, so the material as well as skilled labour is easily available [16].

1.4 Challenges in installation of Concrete Floater

The concept of very large floating structures (VLFS) have been presented in 1920 by Edward Armstrong [17]. In 2001, Japan studied and constructed the first mega float structure which was long floating runway near Tokyo Bay as shown in Figure 1-3. For very large structures, the challenge is to do the maintenance for lifetime of that structure. The main challenge is that horizontal forces on the big structures are very large so the mooring connection must be strong enough to keep the structure at the designed location. In catenary mooring system, these horizontal forces have been tackled by inertial forces. So in this case horizontal size of the structure should be larger than the given wavelength. This will reduce the tension forces in the moorings [18].

Although the horizontal force increased on the large structure which increases the structure motion but on the other hand when structure size increased the added mass, inertial force and restoring forces also increases which enhance the structure stability and as a result the structure motion also reduces.

Figure 1-3 Floating runway Japan [19]

In large steel floating structures like support structures for high rated wind turbines, the main problem is to avoid the corrosion of the steel during its almost 20 years of life span. The higher maintenance and operation cost is required for this purpose. The geometrical shape also plays important role in stability when floating structure encounters the waves, currents and wind.

When the concrete floating substructure is in design process, the main challenge is the hydrostatic pressure especially for spar type structure. The spar has depth around 120 m or more, so the hydrostatic pressure is correspondingly very high. To counterbalance this high pressure with the concrete wall thickness is bit difficult. This high hydrostatic pressure can be reduced by changing the floater type to semisubmersible or barge type. In barge the depth of floater is about 10-15 m while in semisubmersible the draft is about 20-30 m. This can reduce the high hydrostatic pressure.

Figure 1-4 Offshore wind turbine platform corrosion [20]

The other challenge is water leakage in between the different panels as well as water permeability through the walls. Pre-stressing can be used to encounter the bending moment in the walls and this will reduce the permeability through the concrete walls [19].

In concrete floating platform, the main challenge is the reinforcement corrosion which increases the chances of concrete structures deterioration. The parameters which cause corrosion are concrete cover thickness, concrete permeability, chloride content, environmental factors like temperature, cracks and water to cement ratio. The major problem in the concrete construction is to maintain the construction quality which must be good and uniform for whole structure. The other challenge for floating structures especially steel offshore platforms has encrustation of different marine organisms on the surface of the platform as shown in Figure 1-4. This leads to the corrosion of the surface and causes failure and needs regular maintenance [20].

Coupling of wind turbine with the concrete platform is another challenge to stabilize the platform. This can be achieved by changing the floater geometry as well as size of the platform.

Currently, 2 MW and 5 MW floating structures are already proposed, installed and operational at various sites. One method is upscaling of existing floaters for 10 MW or higher which can save the time. The focus of this research is to propose the floater for the coast of Japan and until now almost all the proposed floaters are commercial floaters and it's difficult to start the upscaling of the existing floaters. The second reason is aerodynamic behaviour of 2 MW and 10 MW is not on the linear scale, it effects the floater motion a lot. Although recently few researchers worked on the upscaling of the floater size from 2 MW to 5 MW and 10 MW and proposed some methods but it's still under discussions [21-22].

1.5 Objective

The objective of this study is to propose the innovative design for 10 MW multi-column FOWT made of concrete for the coast of Japan.

1.6 Outline of the Dissertation

In this thesis, hydrodynamic and aerodynamic behaviour of floating offshore wind turbine are presented. This thesis comprises of seven chapters.

Chapter 1: A general situation about wind energy, supporting platform and wind turbine are presented. Offshore wind energy in Japan is also explained. This chapter states the research motivation and objectives.

Chapter 2: Detailed literature review based on different kind of floating platform and improvement of wind turbines by different researchers and its usage are explained. Performance of wind turbine under different water depth is explained and importance of this effect for the electricity generation is also discussed.

As in this research, the purpose is the design of substructure so major focus will be on the supporting platform. 1st , wind turbine main components are described and later on different floating concepts has been explained.

Chapter 3: In this chapter, a case study of FloatGen from Ideol has been explained. A finite element tool COM3 has been used to check the structure behavior under cyclic loading. Tower load and mooring load has been applied and prestressing is also applied.

Chapter 4: In this chapter, conceptual design of concrete floating substructure for 10 MW offshore wind turbine is proposed under static load conditions. This first phase of design is based on the concepts from the case study. The purpose of doing this is to get the basic structural dimensions to start the dynamic equilibrium for further study.

Chapter 5: As the objective of this dissertation is to propose the design of floating substructure to support 10 MW floating offshore wind turbine, so in this chapter, location, type of reference wind turbine, wind conditions, wave conditions have been explained. Also, structure geometry, input and output at equilibrium as well as hydrostatic stability of the proposed floater is explained.

Chapter 6: In this chapter, hydrodynamic behaviour has been evaluated for the shortlisted cases based on parametric study. The turbine used for these simulations is 10 MW IEA reference wind turbine. The hub height above mean sea level is 129 m with rotor diameter of 178.3 m. The proposed structures are examined under different sea conditions while checking hydrodynamic behaviour in WAMIT and under different wind and wave conditions in checking aerodynamic behaviour in FAST.

Chapter 7: In this chapter, model test of the shortlisted case has been explained in the wave tank. The 1:60 scale were conducted to evaluate the hydrodynamic response of the proposed structure under different heave plates position. The structure response was checked under regular waves, irregular waves and transient waves.

Chapter 8: Conclusions of all chapters and future recommendations have been proposed in this section.

Chapter 9: In this chapter references used in the dissertation have been presented.

2 Literature review

2.1 Overview of FOWT

In this chapter, detailed literature review based on different kind of floating platform and improvement of wind turbines by different researchers and its usage are explained. Performance of wind turbine under different water depth is explained and importance of this effect for the electricity generation is also discussed.

As in this research, the purpose is the design of substructure so major focus will be on the supporting platform. 1st , wind turbine main components are described, and later different floating concepts has been explained.

2.1.1 Floating offshore wind concept

Floating wind energy concept was first introduced by William Edward Heronemus in 1972 [23]. Recently, floating offshore wind concept is most popular out of all energy production resources. The first ever large floating offshore wind concept which is also known as Hywind project was launched by Statoil as a spar floater [24]. In this project the reference wind turbine was 5 MW wind turbine. Hydrodynamics and aerodynamics behaviour has been analysed as well as wave induced motion with the help of model test has been verified.

The first ever semisubmersible floater for 5 MW wind turbine was proposed by Fulton in 2005 from NREL [25]. Roddier et al. in 2010 proposed the feasibility studies of the WindFloat concept which was a 3-column semisubmersible steel floater for 5 MW wind turbine. These columns are fitted with heave plates. The first WindFloat project was operated by the end of 2019 [26–29].

In 2015, Michailides and Karimirad proposed a new V shape semi-submersible steel floater for 5 MW offshore wind turbines [30]. This semi-submersible floater was proposed based on the feasibility study. The basic criteria were hydrostatic stability based on the righting moment / healing moment. The concept behind was floater need high metacentric height for higher stability but when stability will be larger it will increase the response amplitude operators. So, based on this criteria floater was shortlisted. Then dynamic evaluation has been done to verify the hydrodynamics and aerodynamics. In 2018, for spar floating wind turbine, Li et al. [31] proposed the dynamic response of floater when it encounters the wave energy converters.

In 2018, Ideol proposed the barge type structure which consists of concrete material for 2 MW floating offshore wind turbine [32]. This barge type structure has depth of only 10 m and they successfully demonstrated the hydrodynamic, aerodynamic behaviour. In 2020, Olave olsan lab proposed the OO star wind floater for 10 MW floating offshore wind turbine [33]. This main material of this floater concrete. This is a semi-submersible floater with 4 columns; 1 column under the wind turbine tower and 3 columns for stability and buoyancy. This floater will be constructed by the end of 2022.

In 2020, the University of Maine proposed the concrete floater named as VolturnUS for 15 MW reference wind turbine. This project was done with the collaboration of NREL [34].

The floating offshore wind turbine field is multidisciplinary it involves hydrodynamics, aerodynamics, wind turbine control system and structural design. Borg and collu explained the coupled dynamic modelling for offshore wind turbine by considering aerodynamic, hydrodynamic, mooring deflection, structural deflection and control system [35]. Marten explained the detailed guidelines on scaling methodology of NREL's proposed wind turbine for 5 MW and its application used in the model test [36]. Farrugia et al. explained the effect of wave motions on the rotor dynamics [37]. Salehyar studied the dissipation effect on the wind turbine blades by using quasi static approach [38]. Larsen and Hanson studied and presented the control algorithm for negative damping produced by blades pitch [39].

To tune the wind turbine controller Odgaard et al. used the pareto curve [40]. Jonkman proposed the hydrodynamic module in the FAST tool for fully coupled aero elasto analysis [41]. To analyze the interaction of floating structures with the waves, in 1995, Lee, C.-H proposed the tool named as WAMIT [42].

2.1.2 Background of Fatigue

First time fatigue was discovered in iron. The first finding about metal fatigue has been submitted by Suresh (1998) [43] which was conducted by Julius Wilhelm in 1820, who explored fatigue phenomena on the chains made of iron. He also built a machine which applied the repeated loads of around 100,000 cycles. The interest in exploring the fatigue was increased because of the increase in the use of iron in bridges and railways. August Wöhler (1870) [44] investigated the fatigue phenomena by providing the S-N curve. These are also called as the Wöhler curves. These curves are used to describe fatigue behavior. The curve today is now used to actualize the problem of fatigue damage by lowering the critical stress in a material. He pointed out clearly that fatigue occurs by crack growth from surface flaw until the material capacity is lower than the applied load. Palmgren investigated the design of roller bearings at the Swedish Roller Bearing Industry, he noted and formulated the design principle influencing the dynamic fatigue loads of the roller bearing, which was published it in a German Engineering Journal, Palmgen (1924) [45].

The phenomenon of fatigue in the concrete got intention bit late. Mallet (1991) proposed the 1st fatigue curve for the concrete compression which was presented by Van Ornum [46]. He found that in comparison to the steel which has limit value there is no limit value for concrete fatigue, but he examined that for about 7000 cycles, there is 40% reduction in the fatigue strength of the plain concrete. Hsu (1981) [47] explained that highway systems development in 1920s led to the gradual importance in the concrete fatigue.

Fatigue in the Concrete is an outcome of long-term less amplitude applied force/stress results into many cycles over life span of the concrete structure. This can occur in shear, compression and tension zones and exhibits failure [48]. Some globally recognized codes i.e. FIB Model Code [49], Euro Code [50] and DNVGL-ST-C502 [51] have referred the fatigue in the concrete, the analytical model and standard theory of fatigue have been accepted and utilized in actual life system.

2.2 Wind Turbine components

There are five main components in wind turbines.

I. Nacelle
II. Blades
III. Rotor
IV. Tower
V. Floating Platform

The details of these are as follows

2.2.1 Nacelle

This is the main part of wind turbine system which consists of high and low speed shafts, generator, gearbox, electronic control and brakes. Yaw control system connects nacelle to the tower. This system helps nacelle and rotor to adjust itself in the aligned direction or parallel of wind. There are 2 shafts within nacelle, which are high speed shaft and low speed shaft. As the rotor rotates at 30 to 60 rpm, so it needs a low-speed shaft but on the other hand generator needs to rotate at 1200 to 1800 rpm, so it needs high speed shaft [52–54].

A gear box is located in between rotor and generator to work at rang of rpm. This gear box helps the wind turbines in changing the rotational speed. Now few turbines use the technology of direct derive generator which can generate electricity even at small rotational speed.

Most of the generator used in wind turbine are AC generator which converts mechanical energy into the electrical energy with the help of blades rotation. Some generators don't need gear box and can run on directly on the rotor speed.

A break system is installed mostly on the high shaft for urgent braking as well as to stop the wind turbine operations at cut out wind speed [55].

The electronic control system controls the wind turbine movement and conditions of turbines. This system changes the nacelle yaw movement, generator loading and blades pitch. The amount of torque generated by rotor can be changed by changing the blades pitch. The purpose of this system is to increase the power output [56].

2.2.2 Blades

Power generation can be increased by increasing the number of blades. Most of the wind turbines have 3 blades but some wind turbines have 2 blades. Weight of 1 blade for 10 MW IEA reference wind turbine is 47.7 tons [57].

2.2.3 Rotor

Rotor consists of 2 or 3 blades and the hub. The performance of wind turbine is largely depending on number of blades length and shape. Rotor may be upwind or downwind design. Most of the wind turbines have three blades with upwind design [58].

2.2.4 Tower

To get the appropriate for the nacelle, tower connects substructure to the nacelle and rotor. The 10 MW reference wind turbine proposed by DTU have the tower height of 119 m [59].

2.2.5 Floating Platform

Floating platform supports all parts of the wind turbines and is connected to the ocean bed with the help of mooring lines most probably catenary type mooring lines. The platform must have sufficient buoyancy to support the super structure. For the extreme offshore environments, there is a big challenge to for the placement of the platform which is stable enough to support tower and rotor nacelle assembly.

2.3 Major technologies in FOWT

There are four main categories in floating wind turbines: Tension leg platform (TLP), Spar, barge and semi-submersible. There are three methods to achieve static stability in all these cases: buoyancy, ballasting and mooring lines. A brief explanation will be presented in this section and details can be seen in [60].

2.3.1 Tension Leg Platform

This platform has a good stability because of tensioned mooring lines that supresses the motions of platform. This concept is proposed by SBM offshore and IFPEN [61] as shown in Figure 2-1. This technology has a big disadvantage that platform installation is difficult as compared to others and if the mooring lines are discontinued then platform stability is a big issue.

Figure 2-1 Tension leg platform design [67]

The advantage of this concept is reduced structural weight due to its compact nature.

2.3.2 Spar

This concept mainly follows the stability due to ballasting principle. Usually it is a vertical cylindrical shape and have large draft. The major portion of the mass lies at the bottom side of the spar. The reason is to lower down the center of gravity as much as possible. The remaining portion of the structure helps in maintaining the buoyancy. Hywind proposed the most advanced Spar shape [62]. Hywind installed the pilot project of five 6 MW FOWT in 2017 which are currently operating in Scotland as shown in Figure 2-2a. In terms of fabrication and stability this concept has a big advantage over others but installation of such a big structure with high rated wind turbine is difficult and it requires larger water depth.

2.3.3 Barge

In this type, water depth is shallow as compared with spar. In this concept, stability is mainly achieved by the larger waterplane area which provides larger buoyancy. This technology has been developed in France in 2018 as Floatgen [19]. First 2 MW wind turbines are in operation off the coast of France as shown in Figure 2-2b. Due to its simple geometry, it can be constructed by using different material as steel and concrete.

a) Hywind Spar concept [68] b) FloatGen Barge (Ideol) [19]

Figure 2-2 Spar and Barge types of FOWT

2.3.4 Semi-submersible

This concept is majorly used in oil and gas industry and ahead of other concepts in FOWT industry as various projects working on this solution. This platform is relatively easy to install as compared to other projects. The wind turbine can easily be mounted at the quayside and towed to the location and bring to the shore for rehabilitation or decommissioning. This platform is attached to the seabed with the help of catenary mooring lines as compared to taut line. The disadvantage of this type is complex geometry, because of this fabrication is more difficult. Semi-submersible floating platform needs a larger structural mass for stability [10].

The WindFloat project is proposed by Principle Power as shown in Figure 2-3a. The first prototype was installed in Portugal in 2011 and operated for four years [63]. Naval Energies Technology also proposed the semi-submersible floater [64] as shown in Figure 2-3b.

b) WindFloat (Principle Power) [69] b) Naval Energies Technology [70]

Figure 2-3 Floating offshore wind turbine – Semi-submersible concept

2.4 Floating Offshore Wind Turbine Mechanics

In this section, brief introduction for the basic theory to understand the hydrostatic and hydrodynamic analysis has been explained. The aerodynamic behaviour of the FOWT is also studied in this chapter.

2.4.1 Degree of freedom and coordinate system

The degree of freedom and coordinate system is shown in Figure 2-4. The translational movement parallel to x-axis is defined as surge and translational movement parallel to y-axis is known as sway. Heave is the translational movement parallel to z-axis. The rotation around x-axis is roll and the rotation around y-axis is pitch. The rotation around z axis is yaw.

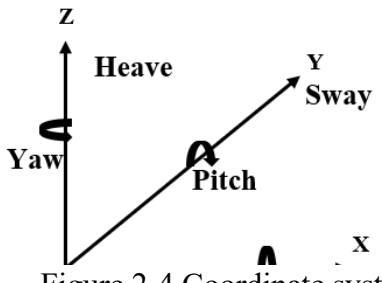

Figure 2-4 Coordinate system

2.5 Floating platform

2.5.1 Buoyancy and Gravity system

By Newton's 1st law, equilibrium of the floating platform is achieved by using the structure weight and buoyancy from the water. Buoyancy follows the Archimedes rule which explains the completely or partly submerged structure can float if force from the water on the structure is equal or higher than the weight of the structure [65]. Equation 2-1 shows the relation between buoyancy force and gravity force in different directions.

$$F_B - F_G = \rho g V - mg = 0 \qquad 2\text{-}1$$

Weight of wind turbine system comprises of platform weight, ballast, mooring line, tower and rotor nacelle assembly. For calculating the center of gravity, the individual parts location is important. The center of gravity can be calculated as equation 2-2. $COG_x = \frac{\sum_n (x_n \, \mathrm{d}m_n)}{\sum_n \mathrm{d}m_n}$ 2-2

Center of buoyancy is dependent on the weight of the structure which displaces the water by equal volume. For semi-submersibles, it can be found by multiplying center of each part by the volume of that part and divided by volume displaced as shown in equation 2-3.

$$COB_y = \frac{\sum_n (y_{bn} \, \mathrm{d}V_n)}{\sum_n \mathrm{d}V_n} \qquad 2\text{-}3$$

2.5.2 Hydrostatic stability

A stable floating body is the body which upon tilting returns to the equilibrium. For a semisubmersible, the point G, center of gravity where body weights concentrate, must lies above the point B, center of buoyancy where center of displaced liquid acts as show in Figure 2-5.

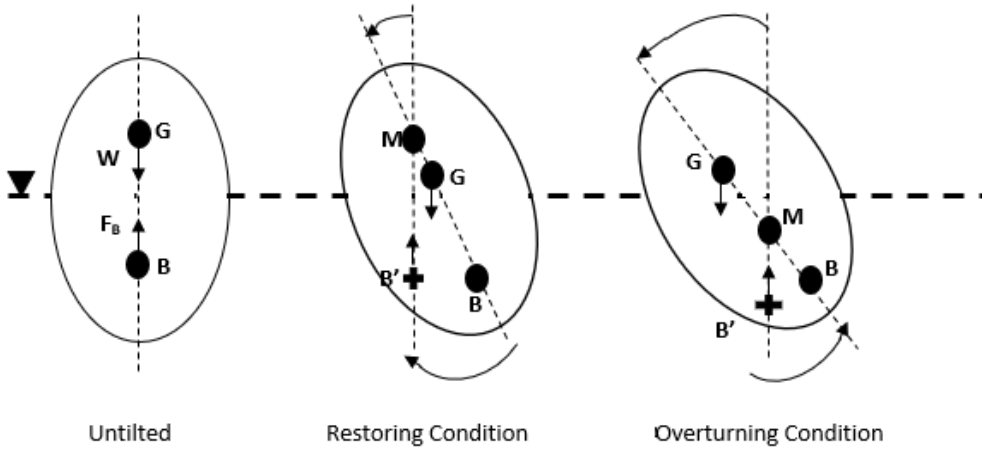

Figure 2-5 Floating bodies stability conditions

Upon tilting, buoyancy center, B, shifted to B' location because of shifting of displaced volume of liquid. A new position M, which is metacentre, is defined. M is the point where vertical upward projection of new buoyancy center B' intersects the centreline. The configuration of Fb and W in the center diagram gives the restoring condition which rotates the tilted body back to its position. In the right-side diagram, FB and W gives the overturning condition which rotates the tilted body away from equilibrium. We can

conclude that when M lies above G, the body will be in stable condition and vice versa. If metacentric height, GM, is positive or GM > 0, the floating body will be stable, and it will be unstable when GM < 0 as shown in Figure 2-6.

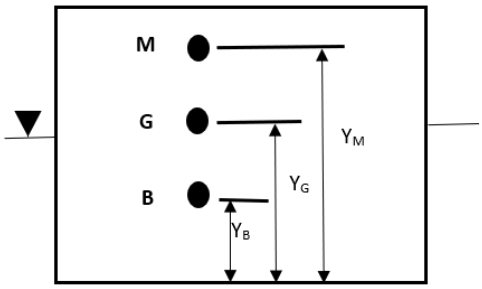

Figure 2-6 Metacentric height GM

From here, metacentric height, GM, is given by Equation 3-4.

GM = MB – GB or

$$GM = \frac{I}{V} - GB \qquad 2\text{-}4$$

Where I is the moment of inertia of plan section, V is sinking volume of the floating body and GB is distance from buoyancy center to gravity center.

2.5.3 Equations of motions

For floating body, equations of motions were stated by Newton's second law. These can be written as [66]:

$$\sum_{k=1}^{6}. M_{jk}\ddot{\eta}_k = F_{jk} \qquad 2\text{-}5$$

The applied load or force on the structure can be denoted by Fjk. This can be divided into two parts shown in Equation 2-6. The one part is force due to the motions of the floating structure while another is because of the motions of the nearby surrounding waves. Force due to motions of the structure can be represented in Equation 2-7 while force due to the nearby surrounding waves can be calculated by Equation 2-8.

$$F_{jk} = F_{Jk}^{sm} + F_j^{wm} \qquad 2\text{-}6$$

$$F_{j_k}^{Sm} = A_{jk}\ddot{\eta}_k + B_{jk}\dot{\eta}_k + C_{jk}\eta_k \qquad 2\text{-}7$$

$$F_j^{wm} = F_{j_0}\, cos\left(\omega_e t + \varepsilon_j^F\right) \qquad 2\text{-}8$$

Here, j and k denote the six degrees of freedom and same values of j and k represents the behaviour of motion in single degree of freedom. Unequal j and k mean there can be coupling between degree of freedom. Added mass, damping and restoring forces coefficients can be represented by A_{jk}, B_{jk} and C_{jk}.

By combining Equations 2-7 and 2-8 into equation 3-6, we can rewrite as:

$$F_{jk} = \left(Mjk + A_{jk}\right)\ddot{\eta}_k + B_{jk}\dot{\eta}_k + C_{jk}\eta_k \qquad 2\text{-}9$$

Mass matrix is shown here as M_{jk} while added mass matrix is shown as A_{jk}. Damping matrix represented here as B_{jk} and stiffness matrix is shown as C_{jk}. In matrix form, equation can be re write as:

$$F = \big(M + A(w)\big)\ddot{\eta} + B(\omega)\dot{\eta} + C\eta \quad 2\text{-}10$$

2.5.4 Floating body Natural Frequency

Eigenvalue problem can help us to calculate the natural frequency of floating bodies without excitation and damping and can be seen in equation 2-11.

$$(-\omega^2(M + A(\omega) + C)\eta_0) = 0 \quad 2\text{-}11$$

$$\det\left((-\omega^2(M + A(\omega) + C)\eta_0\right) = 0 \quad 2\text{-}12$$

For different degree of freedom, the expression can be written as shown in Equation 2-11

$$\omega_{nj} = \sqrt{\frac{C_{jj}}{Mjj + Ajj(w)}} \quad 2\text{-}13$$

2.6 Floating structure loads

There are two different types of loads on the floating platform; static loads and dynamic loads. The static loads include hydrostatic loads, gravitational loads, equipment's loads. While dynamic loads are due to wind and waves.

2.6.1 Hydrostatic pressure

The portion of the floating body that is submerged bears the hydrostatic pressure. For spar type structure, hydrostatic pressure is higher as compared to the semisubmersible as the depth of semisubmersible is smaller as compared to the spar.

2.6.2 Diffraction and radiation

To understand wave loads, diffraction and radiation are essential terms. If we place a structure inside water, the structure will be encountered by waves. If the structure is of good size and weight, it also affects the surrounding waves. This phenomenon is known as radiation and diffraction. In radiation, the structure is pushed to oscillate with the same frequency as of waves. The loads in radiation problem are damping, added mass and restoring force. The wave-radiation loads include contributions from hydrodynamic added mass and damping. The wave radiation loads are independent of the incident waves. These mainly depends on floater body geometry. Added mass is the weight added to a system as an accelerating or decelerating body must move some volume of surrounding fluid with it as it moves.

The total damping is separated by potential damping and viscous damping.

- The damping calculated by potential is called the wave building damping force, which generates waves around the floating body as it moves and is linearly related to the wave height.
- Viscous damping cannot be calculated by potential (e.g., by free oscillation test using a model in a water tank) and is nonlinear with wave height.

In In diffraction, the structure is supposed to be fixed against moving with waves and is evaluated by waves excitation force. These wave excitation forces are divided into 2 categories: Froude-Krylov forces and diffraction forces. Froude-Krylov forces are from pressure field due to undisturbed wave applying loads on the floating structure. The

diffraction forces or scattered forces are because the floating structure changed the pressure field

2.6.3 Morison's equations

The empirical equation to calculate the drag forces and inertia forces applying on the floating body which is exposed to wave loads.

For basic fixed cylindrical column, Morison's equation can be expressed as:

$$\hat{F} = \frac{1}{2}\rho C_d D|u|u + \rho C_m A\dot{u} \qquad 2\text{-}14$$

Where

$\hat{F}$ = Force per unit length of member

Cd = Drag coefficient

Cm = Inertial coefficient

ρ = density of sea water

D = diameter of column

A = cross-sectional area of column

u = velocity of the wave at right angle to the structure

$\dot{u}$ = acceleration of the wave at right angle to the structure

3 A Case Study - FloatGen

In this chapter, a case study of FloatGen from Ideol has been explained. A finite element tool COM3 has been used to check the structure behavior under cyclic loading. Tower load and mooring load has been applied and prestressing is also applied.

3.1 First FOWT with RC Floater (FRANCE)

The construction of first barge type concrete floating offshore wind turbine was started in 2017 at Saint Nazair harbour, France. The commissioning was started by mid-2018. The capacity of this turbine was 2 MW. The water depth at the construction site was 33 m. The layout of barge type FOWT can be seen in Figure 3-1.

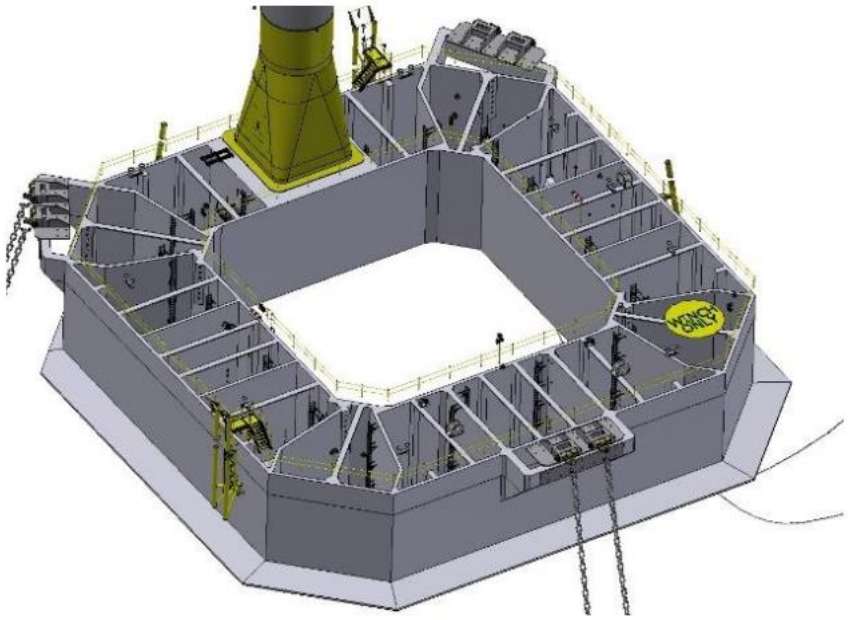

Figure 3-1 Layout of Floatgen Ideol [15]

The overall hull main dimensions are 40 m x 40 m x 9.5 m. The buoyant hull dimensions are 36 m x 36 m x 9.5 m. The width of skirt span is 2.2 m. The synthetic mooring lines have the breaking strength of 8000 KN.

3.2 Finite element tool

The finite element tool used for this purpose is COM3 [67]. To achieve the rational design, construction, and maintenance of concrete structures, it is important to predict the performance of structures over lifespan, from the start of the hydration reaction until the end of their service life, considering various material and mix proportions, structural dimensions, and curing and environmental conditions. Aiming for a unified approach to the evaluation of the behaviour of concrete structures under any of various conditions, the Concrete Laboratory of the University of Tokyo, Japan has been working to develop a multi-scale integrated analysis platform, DuCOM-COM3 can be seen in Figure 3-2.

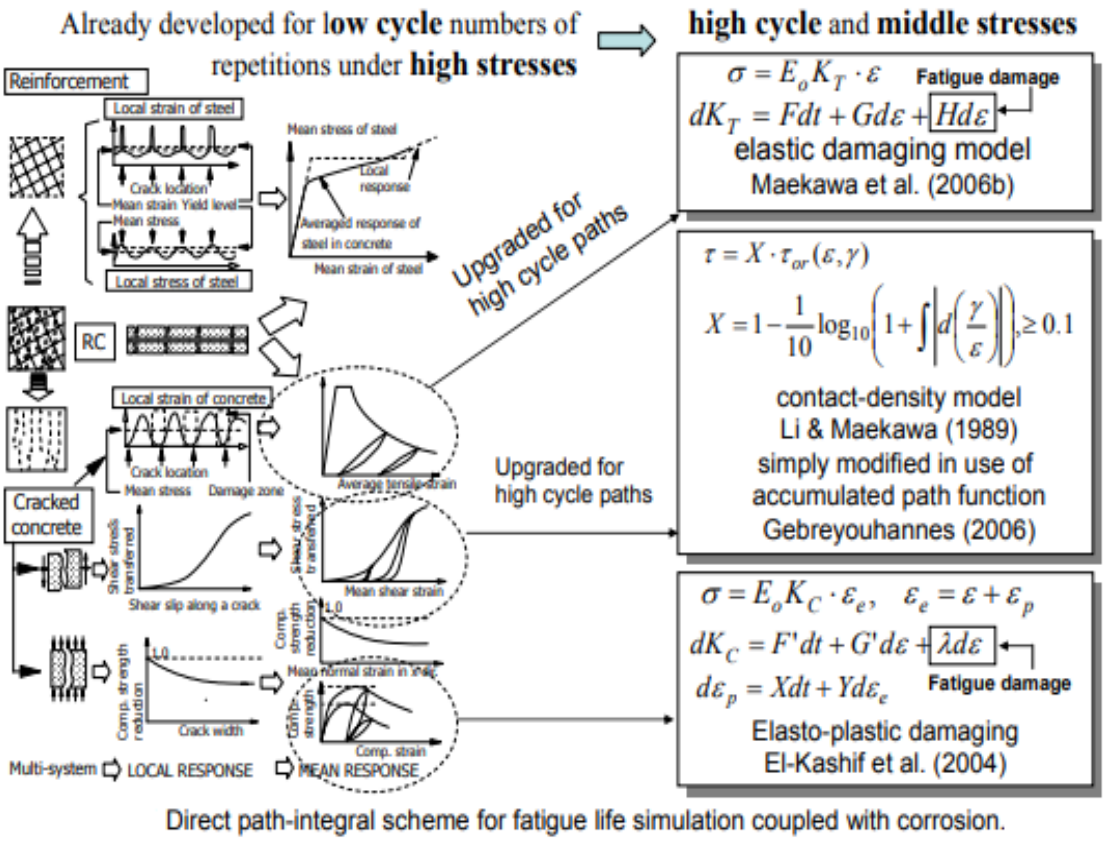

Figure 3-2 Concrete fatigue constitutive model used in COM3 [68]

3.2.1 Load pattern and connection details

The total of 8000 KN of fatigue mooring load is applied to the structure, As these loads are concentrated so, there is a need of distributing this load gradually to the structure. The yield stress of the mooring line was 540 MPa and the mooring connection has the yield stress of 420 MPa which connects to the structure that has the yield stress of 345 MPa [69]. The finite element model and steel connector can be seen in Figure 3-4. For water tightness as well as high bending stress on the wall of structure, it is required that walls should be in tension to avoid the cracking. For this reason, 10 MN prestress load is applied to the structure which is distributed along the depth. Also the prestress load of 10 MN is also applied under tower as shown in Figure 3-3.

As mentioned in Table 3-1, four different models have been considered. The first model is small solid section with mooring loads from 1 side and symmetrical boundary conditions. The second is small hollow section with mooring loads from 1 side and symmetrical boundary conditions. The third is small hollow section with prestress load inside walls and symmetrical boundary conditions. The fourth model is full hollow prestress with the mooring loads from 3 sides as well as restrained in z-direction as well as bottom layer was taken as elastic layer. These models are named as M1, M2, M3 and M4.

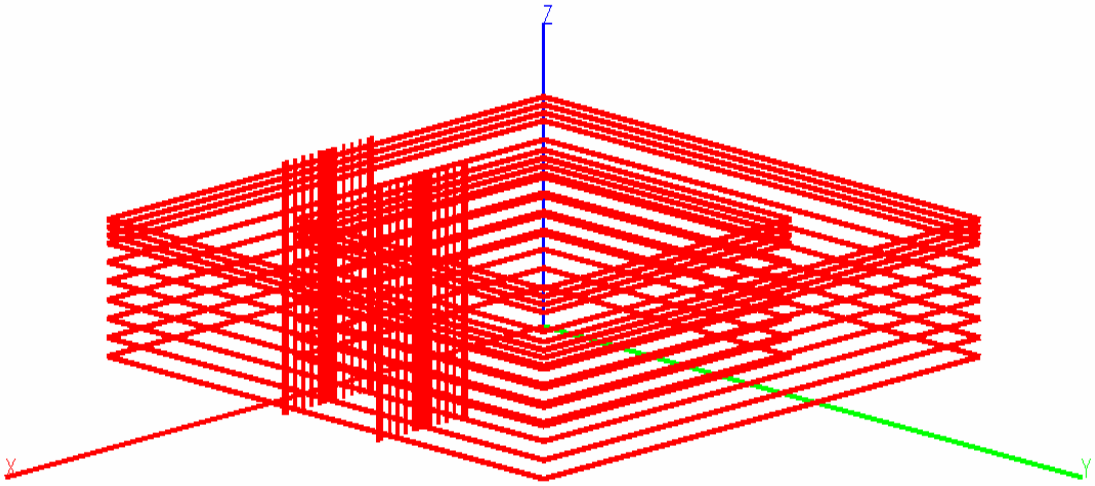

Figure 3-3 Prestress load configuration

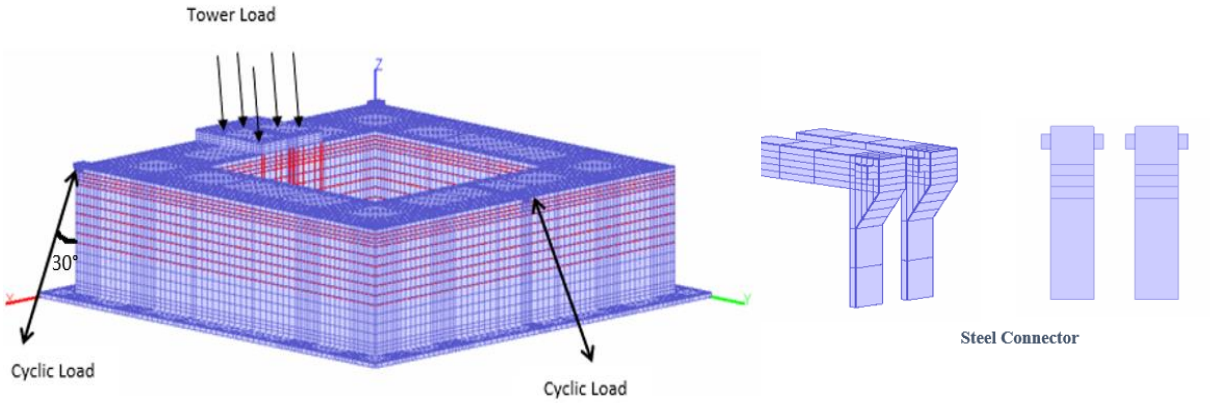

Figure 3-4 FE model and steel connectors of Ideol barge structure

Table 3-1Case study parametric models

Model Name	Type	Load	Boundary Condition
M1	Small Solid Section	Mooring line fatigue load on connector from 1 side	Symmetric B.C
M2	Small Hollow Section	Mooring line fatigue load on connector from 1 side	Symmetric B.C
M3	Small Hollow Prestressed Section	Mooring line fatigue load on connector from 1 side	Symmetric B.C
M4	Full Hollow Prestressed	Mooring line fatigue load on connector from 3 sides	Restrained in z-direction and bottom layer as elastic layer

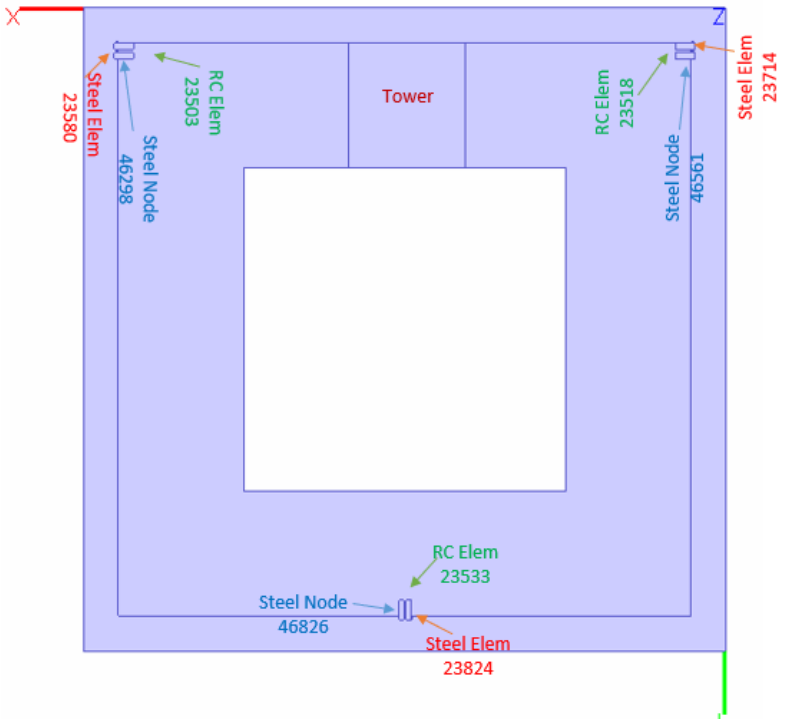

Figure 3-5 Top view of the model and elements description

In Figure 3-5, the arrangements of the elements have been presented. In Figure 3-6, the steel stresses under cyclic load of 2660 KN have been presented. Under different percentage of loading from 100% to 60% of mooring loads. From here it can be noticed that the stresses in the steel connectors are less than the yield stresses taken for the steel connectors.

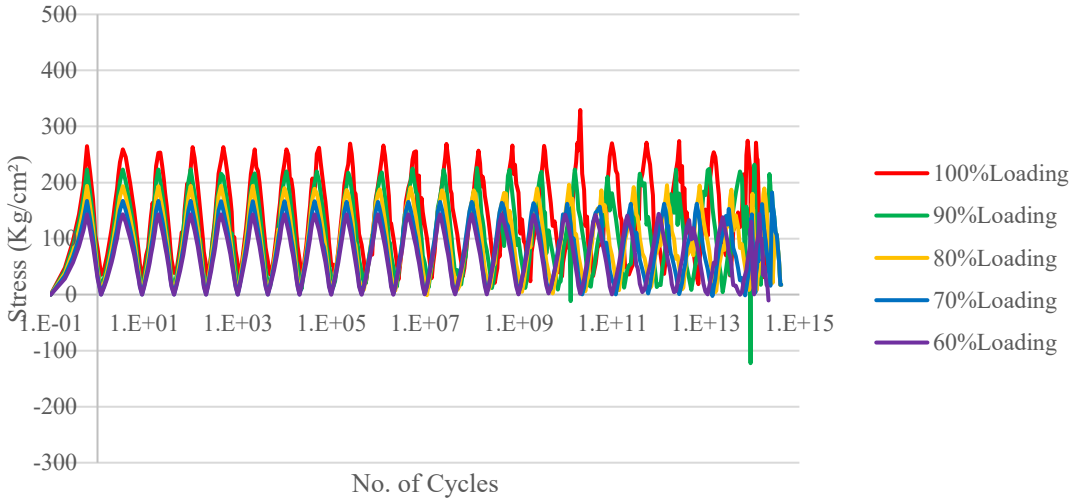

Figure 3-6 Steel Stresses in Mooring connection

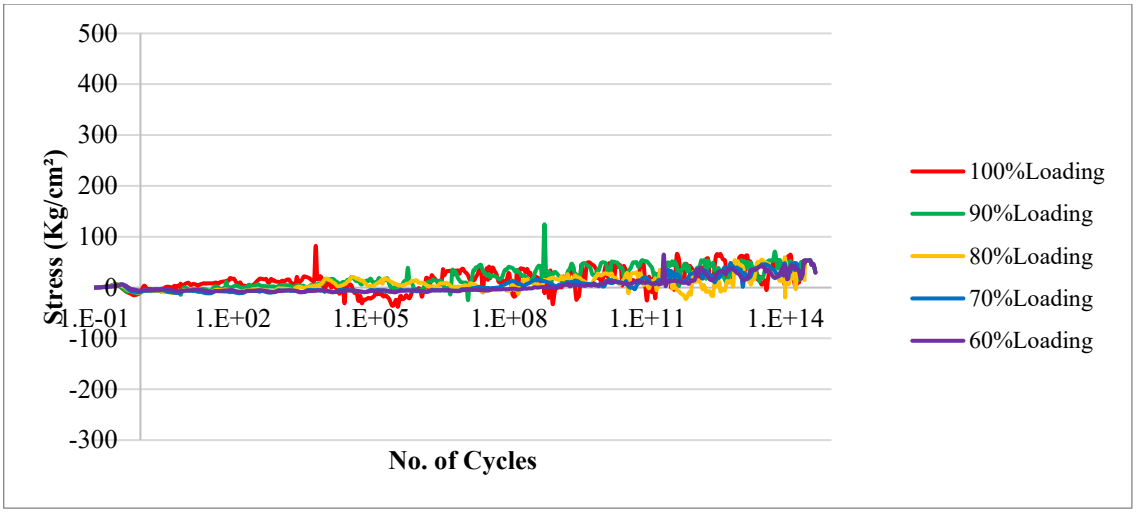

Figure 3-7 Concrete stresses in the element adjacent to the steel connector

In Figure 3-7, the mooring load of 2660 KN under different percentage has been applied to the steel connector and checked the stresses in the adjacent concrete elements. The concrete stresses are very less as compared to the yield strength of the concrete.

3.3 Summary of chapter

The behaviour of 2 MW barge type concrete floater has been checked under static load conditions by assuming the boundary conditions as the buoyancy load from bottom and mooring load from 3 mooring connection. The finite element model COM3 (3-dimensional concrete model) used to check the mooring connection response. Dynamic loadings on the mooring connections have not been considered.

1. Stresses in the steel connections are much below than the yield strength of 420 MPa. This is due to the not considering the dynamic loads as well as wind turbine generator loads in combination.
2. From this case study, the idea of floating structures, hydrostatic stability, Stresses in the connections have been extracted, which helped in this research while proposing the model in next rounds.

4 Design of Panel Based Reinforced Concrete Floating Substructure for 10 MW Offshore Wind Turbine

In this chapter, conceptual design of concrete floating substructure for 10 MW offshore wind turbine is proposed under static load conditions. This first phase of design is based on the concepts from the case study. The purpose of doing this is to get the basic structural dimensions to start the dynamic equilibrium for further study.

4.1 Structural details of concrete floater based on geometric design

In this section, geometrical design of panel based reinforced concrete floating substructure for 10 MW wind turbine generator is based on floating body stability concept. The structural details are given in Table 4-1.

Table 4-1 Structural details of concrete floater

Description	Value
Concrete floater depth	20 m
Buoyant concrete floater width	72 m
Wall thickness	0.7 m
Depth of inner hexagon under tower base	5 m
Top slab thickness	50 cm
Bottom slab thickness	50 cm
Skirt span	2 m
Light weight concrete density	1600 Kg/m³
Compressive strength of concrete	50 MPa

The side length of inner hexagon which directly supports tower is 8 m as shown in

Figure 4-1**,** white equilateral triangle portion is fully hollow, sea water can come inside and go outside freely. Grey portion is inside hollow box with top and bottom slabs. Concrete floater depth and buoyant concrete floater width are decided based on fulfilling the criteria of floating body concept. Here, center of gravity lies above the center of gravity and geometric height is also well above the center of gravity as shown in Figure 4-2.

By increasing the depth and increasing the buoyant floater width, freeboard will also be increased till selected floater geometry after that freeboard increased little bit, but these are highly uneconomical as compared to the selected floater geometry. The floater width

of 48 m, 56 m, and 64 m are not suitable because of no or very small freeboard availability. The first suitable and economical floater dimensions are: buoyant floater width of 72 m and floating substructure depth of 20 m because of freeboard availability of 2 m and draft of 18 m as shown in Figure 4-2.

Table 4-2 Geometrical properties of RC floater

Buoyant Floater Width B	Side Length L	Floater Depth d	Draft	Freeboard	COB	COG	GM
112	56	10	7.6	2.4	3.8	8.2	158
104	52	12	9.0	3.0	4.5	9.2	116
96	48	14	10.6	3.4	5.3	10.2	83
88	44	16	12.6	3.4	6.3	11.3	58
80	40	18	15.0	3.0	7.5	12.3	40
72	**36**	**20**	**18.0**	**2.0**	**9.0**	**13.4**	**26**
64	32	22	21.6	0.4	10.8	14.5	16
56	28	18	21.7	-3.7	10.8	14.0	11
48	24	16	23.7	-7.7	11.8	14.4	7

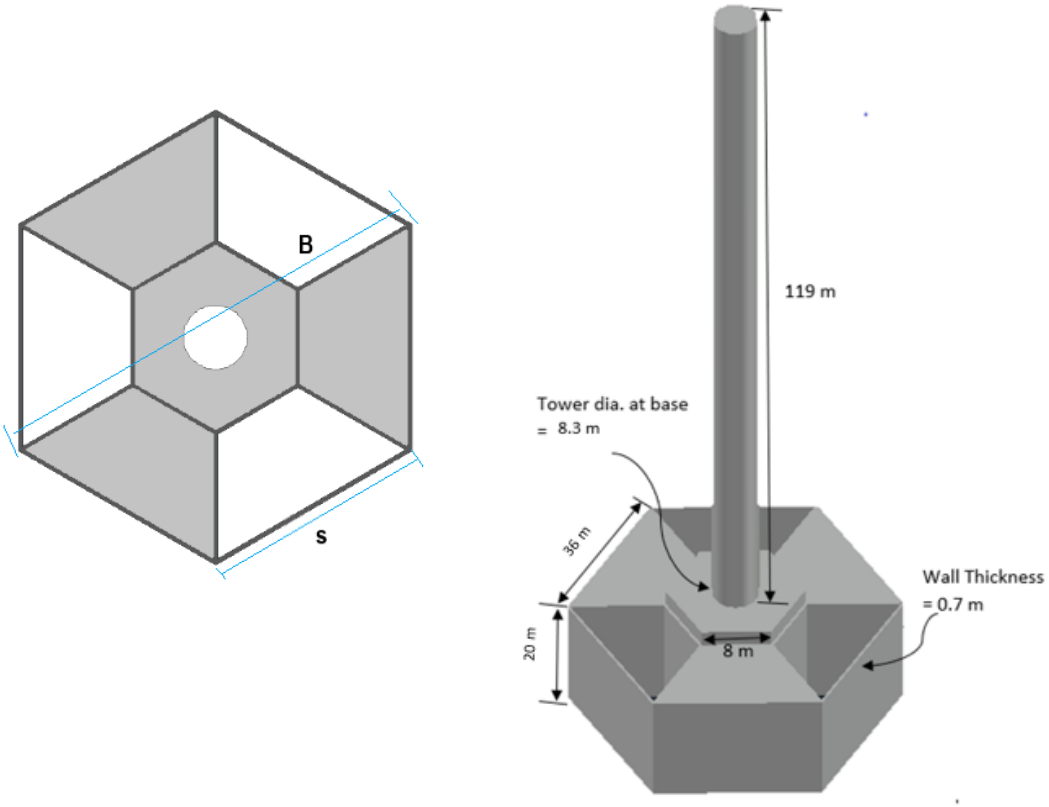

Figure 4-1 Proposed reinforced concrete floater

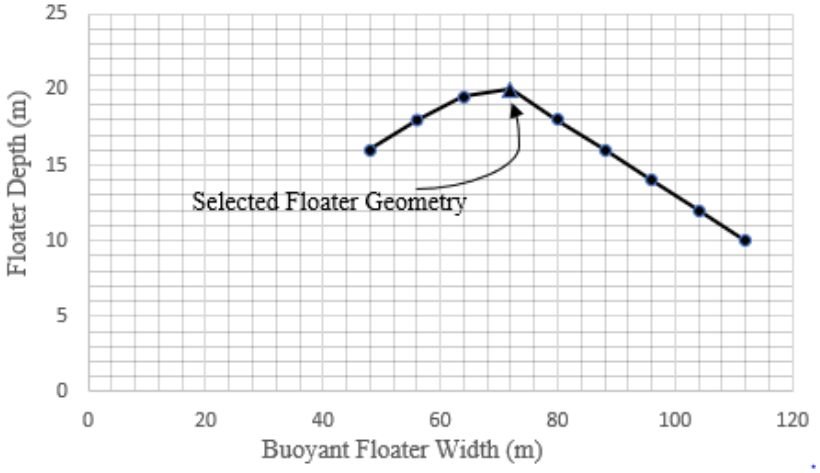

Figure 4-2 Optimum geometric comparison

4.2 Structural design

Light weight aggregate concrete of density 1600 Kg/m³ and compressive strength of 50 MPa is assumed.

4.2.1 Tower to Floater Connection Part

To design the concrete floater portion connected to tower base, wind load based on wind speed 25 m/s is taken on the top of tower. Required reinforcement ratio is calculated by using ACI equation 10.3.

$$\rho = w\left[1 - \sqrt{1 - \frac{2.614R}{fc'}}\right] \tag{4-1}$$

Here,

$$R = \frac{Mu}{bd^2}$$

$$w = 0.85\frac{fc'}{fy}$$

ρ = reinforcement ratio

Mu = ultimate moment

fc' = concrete compressive strength

fy = yield strength of steel

b = cross-sectional width

d = cross-sectional depth

Minimum area of steel governed because of the larger concrete area as given in Figure 4-3. To accommodate Asmin of 1072040 mm2, 2800 – 22.0 mm dia. @ 150 mm clear spacing will be provided.

Design of anchor bolt for concrete pull out or breakout depends on uncracked concrete versus cracked concrete. To avoid the tower base pulling out from the concrete floater, special anchorage has been designed as shown in Figure 4-4a. For this purpose, by using A36 bolt and plate SS400 [70], 86 number of anchor bolts have been provided with the clear spacing of 30 cm. The diameter of anchor bolt is 3.8 cm and embedded length is 120 cm. When anchor bolts anchored in concrete, upon pulling out / failure a conical shape is formed around 45° as shown in Figure 4-4b. Shear reinforcement is also provided to stop the crack propagation.

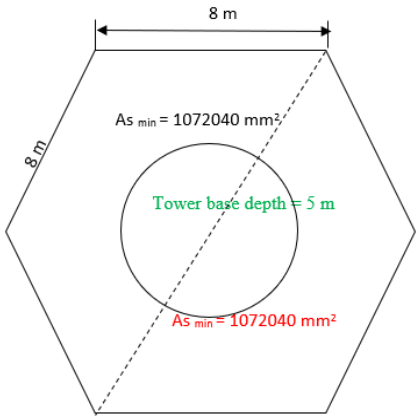

Figure 4-3 Reinforcement under Tower base area

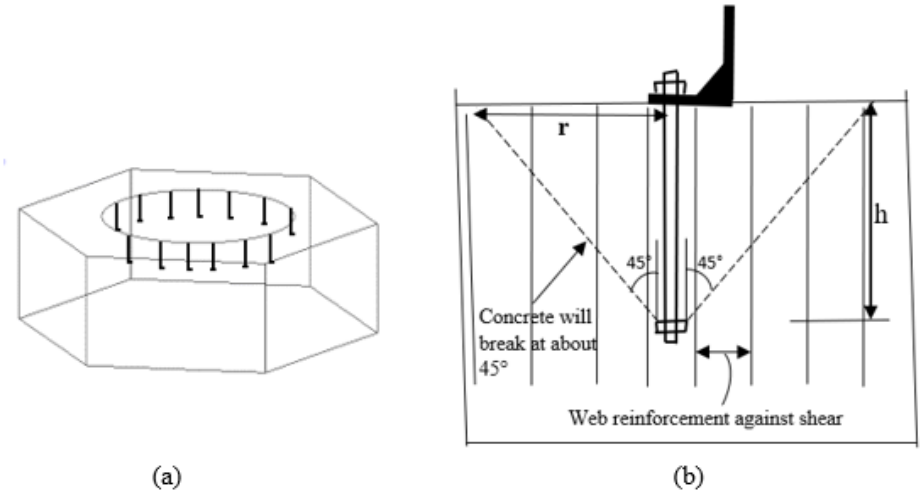

Figure 4-4 Anchorage at tower base

4.2.2 Slab Design

Slab is designed under self-weight and live load. The two-way slab is designed by using ACI coefficient method. ACI equation 9-12 is used to calculate minimum depth of the reinforced concrete slab.

$$hmin = \ln\left(\frac{0.8+ {}^{fy}/_{1500}}{36m+9}\right) \quad (4\text{-}2)$$

Thickness of the slab is decided as 50 cm which is greater than required thickness of slab. The cover is taken as 70 mm. As concrete area is big, minimum area of steel governed which is 900 mm²/m as shown in Figure 4-5. Here, 900 mm² is 13 mm diameter bars @ 140 mm clear spacing in both directions.

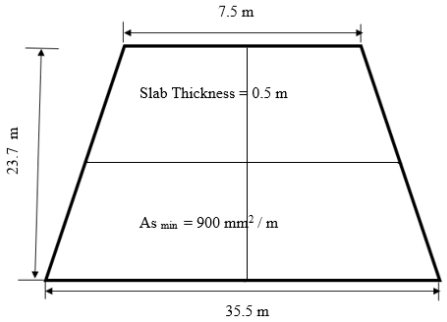

Figure 4-5 Slab reinforcement

4.2.3 Wall Design and crack width criteria

The side wall is designed under serviceability limit state. The applied moment is taken from the hydrostatic pressure at 1/3rd height from the bottom of the floating substructure. According to JSCE guidelines [71], the concrete cover for splash zone is given for concrete permeability of 10-12 m^2/s is 70 mm. By fulfilling the criteria of flexure from ACI 318-08 [72] equation 7.3 and shear from ACI 318-11 equation 11.2.1.1 [73], thickness of the side wall is taken as 700 mm as shown in Figure 4-7.

$$\text{hs for flexure} = \sqrt{\frac{M}{0.175 b f_c'}} \tag{4-3}$$

Here,

M = applied moment

fc' = concrete compressive strength

b = cross-sectional width

This is modified equation for light weight concrete with compressive strength of 50 MPa. The required minimum thickness of the wall for flexure is 425 mm.

$$\text{hs for shear} = \frac{V}{0.75 * 0.17 \sqrt{f_c'} b} \tag{4-4}$$

Here,

V = applied shear

fc' = concrete compressive strength

b = cross-sectional width

The required minimum thickness of wall for shear is 270 mm. The calculation of required area of steel for compression zone as well as for tension is done by using equation 2. Area of steel for tension zone is 83820 mm^2 and for compression zone is 40660 mm^2 as shown in Figure 4-7. 255 – 22 mm diameter rebars @ 130 mm clear spacing in 2 layers are provided in tension zone and 110 - 22 mm diameter rebars @ 160 mm clear spacing are provided in compression zone. Equation 10-4 (ACI 318-08 [72]) is used to calculate maximum spacing. From this equation, the required maximum rebar spacing is 898 mm and given rebar spacing is 130 mm.

$$smax = 380.\frac{280}{fs} - 2.5\,c \quad (4\text{-}5)$$

Here,

fs = steel stress

c = concrete cover

By utilizing the concept of allowable service state, depth of neutral axis is 160 mm which is calculated by using the concept shown in Figure 4-6. It means out of 700 mm thickness of the wall; 160 mm is the compression zone and 540 mm is the tension zone. When the hydrostatic pressure or water load is applied from the outside of the wall, mainly compression zone plays its role as concrete is very good in compression or we can mention that it's difficult for crack opening or crack propagation in compression zone. This is the reason compression zone depth must be sufficient to bear the crushing behaviour of applied load and minimize the effect to transfer in the tension zone. In tension zone, due to the bending behaviour of hydrostatic pressure may be few cracks will appear, but these cracks are within permissible range. The advantage of hollow box type concrete floater is that there is no sea water inside the hollow box. Even cracks initiated within permissible range, these will not be harmful same as onshore structure.

By using ACI 224.1R-07, equation 1-1[74], the crack width is 0.129 mm. In JSCE section 8.3.2, crack width opening criteria for splash zone is 0.0035c. From here, allowable crack width is 0.245 mm which greater than calculated crack width.

$$w = 2.\frac{fs}{Es}.\beta.\sqrt{dc^2 + (\frac{s}{2})^2} \quad (7)$$

Here,

$$\beta = \frac{h - c}{d - c}$$

Here,

fs = steel stress

Es = modulus of elasticity of steel

dc = distance from outer surface to the center of exterior rebar

s = rebar spacing

h = cross-sectional depth

c = concrete cover

For compensating the permissible crack width, given rebar spacing is lesser than maximum rebar spacing, and applied service moment is lesser than cracking moment.

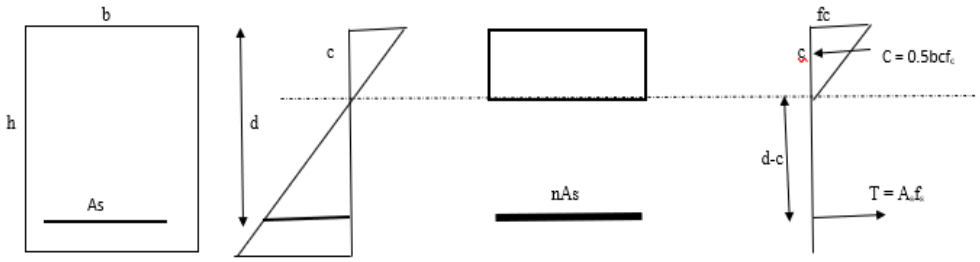

Figure 4-6 Neutral axis and compression zone

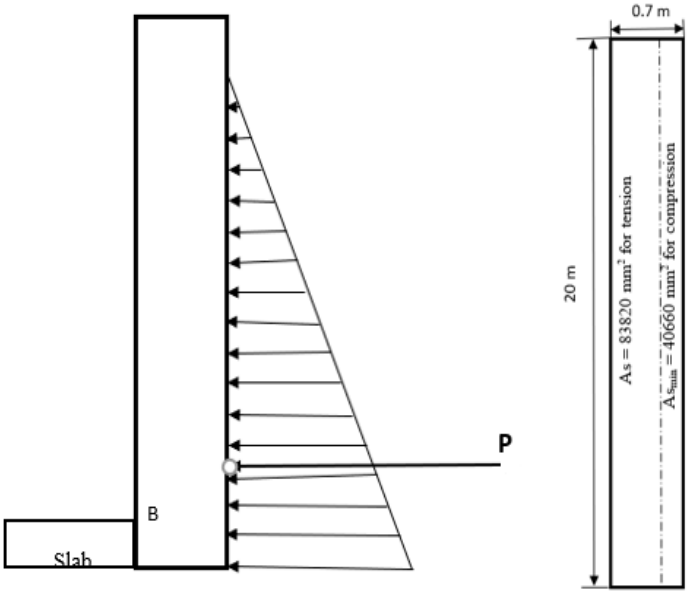

Figure 4-7 Side wall design

4.2.4 Mooring Line to Floater Connection

Mooring line to concrete floater connection is designed based on fulfilling the bearing strength of plate, plate thickness, welding, number of anchor bolts, resistant uplift check, combined tension and shear check and base plate thickness. The breaking load of 1600 t is the cluster of mooring lines are taken from the typical breaking load of 6 MW floating wind turbine [75]. The exact mooring load will be calculated on the later stage of this research. To spread the concentrated mooring load to the concrete floater, different yield stress of the steel has been considered. The finalized mooring to concrete floater dimensions is shown in Figure 4-8.

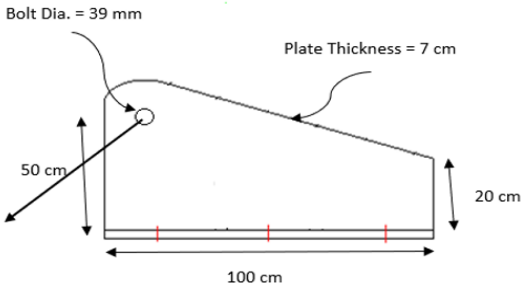

Figure 4-8 Mooring connection for concrete floater

4.3 Summary of chapter

The conceptual design of concrete floater for 10 MW floating offshore wind turbine has been proposed under static load conditions. This first phase of design was based on the concepts from the case study. The basic idea to propose this shape will be easy in mass production of precast construction. So, the reinforced concrete pre-cast panel-based construction was assumed.

- Hydrostatic pressure is 181 KN/m for unit strip which is smaller than the hydrostatic pressure in spar of 120 m draft where it is 1207 KN/m.
- 5 m thick concrete portion has been proposed under the tower connection to accommodate the wind turbine generator loads.
- 2600 KN Mooring load has been considered to design the mooring connection.
- In 1st stage under static loading, the tower connection thickness was 5 m to accommodate the 10 MW wind turbine generator loadings and vibrations. 2800 – 22 mm diameter @ 150 mm clear spacing has been provided to resist the bending moment. To prevent the tower base dragging out from the floating concrete structure, exclusive anchorage has been provided. For this reason, A36 bolt and plate SS400, 86 anchor bolts was arranged with a spacing of 30 cm. The anchor bolt diameter is 3.8 cm, and it was embedded up to 120 cm.
- Slab thickness is taken as 50 cm that is larger than needed slab thickness. The required concrete cover is 70 mm. For larger concrete sections, minimum area of steel governed i.e. 900 mm^2/m. As a result, at a clear spacing of 140 mm, 13 mm diameter bars in both directions have been arranged.
- The minimum required thickness of wall is 270 mm for shear. In tension zone, 255 – 22 mm dia. bars @ 130 mm clear spacing in 2 different layers are provided and in compression zone 110 - 22 mm diameter rebars @ 160 mm are provided.
- Out of 700 mm wall thickness, 160 mm was calculated as compression zone as the depth of neutral axis is 160 mm under allowable service design. The tension zone depth is 540 mm. The minimum depth of compression zone is necessary to bear the crushing effect of outside hydrostatic as well as hydrodynamic loadings. So as result, there may be few cracks in tension zone but these cracks are lesser than the allowable crack width.
- By using ACI 224.1R-07, the crack width is 0.129 mm. In DNVGL-ST-C502, allowable crack width is 0.2 mm. From here, allowable crack width is 0.2 mm which larger than computed crack width.
- In the parametric study, wall thickness, slab thickness, tower connection thickness has been adopted from this preliminary design.
- This structure hydrodynamic behaviour has been checked in the next phase, but response was not good. Then the structure is modified.

5 Multi-Column Semi-Submersible Design Mission

As the objective of this dissertation is to propose the design of floating substructure to support 10 MW floating offshore wind turbine, so in this chapter, location, type of reference wind turbine, wind conditions, wave conditions have been explained. Also, structure geometry, input and output at equilibrium as well as hydrostatic stability of the proposed floater is explained. The initial dimensions are assumed based on the preliminary structural design.

5.1 Premises

5.1.1 Location

Location for this study is the Japanese ocean as the sea environmental conditions are severe here and intension is to use this floater in the Sea of Japan and Pacific Ocean.

5.1.2 Depth

Ocean depth varies as we move away from the coast. Till now, concrete semisubmersible floaters are proposed up to the depth of 130 m. In this research, the depth of concrete semisubmersible is taken as 200 m.

5.1.3 Reference Wind Turbine

Design of tower, rotor nacelle assembly is out of capacity of this research, so a predefined wind turbine generator properties and analysis were used. The International Energy Agency (IEA) 10 MW wind turbine generator [76] was adopted as a reference in this research so that the design of floating substructure should be done accordingly. The key characteristics are shown in Table 5-1. The rated wind speed is 11 m/s, cut-in and cut-out wind speeds are 4 m/s and 25 m/s, respectively. The purpose to develop the IEA 10 MW reference wind turbine was to evaluate the aerodynamics and rotor performance, aero and elastic behaviour and control system of turbine but the parameters which will be used in designing the floating substructure are also proposed. The detailed parameters can be seen in the IEA 10 MW document [76].

5.1.4 Wave conditions

Three sea conditions from the proximities of the Japanese coast were selected, namely operational, storm and centenary conditions.

The irregular wave characteristics can be represented by the International Ship and Offshore Structure Congress (ISSC) spectrum [77]. The wave spectrum for the different sea states with their respective period of peak, Tp, and significant wave height, Hs, are shown in Table 5-2.

The wave spectrum of three wave conditions i.e. operational, storm and centenary on the Japanese coast are shown in Figure 5-1. In this research, main focus is to verify the floating structure under operational sea conditions.

Table 5-1: Wind Turbine Generator Properties

Description	Value
Rating	10 MW
Rotor orientation	upwind, 3 blades
Control	Collective pitch, Variable speed
Hub Diameter, Rotor diameter	5.6 m, 178.3 m
Hub Height	119 m
Cut-in, average wind speed, cut-out	4 m/s, 11.4 m/s, 25 m/s,
Drivetrain	Medium speed
Rotor speed, Cut-in	9.6 RPM, 6 RPM
Rated tip speed	90 m/s
Pre-bend	3 m
Blade Mass	47.7 ton each blade
Nacelle Mass	639 tons
Tower Mass	539 tons

Table 5-2 Wave Conditions

Condition	**Wave Significant Height, H_S**	**Wave Peak Period, T_p**
Operational	2.5 m	9.0 s
Storm	9.6 m	13.5 s
Centenary	4.0 m	16.1 s

5.1.5 Wind conditions

Three different wind conditions were selected as maximum operational, cut-out and typhoon conditions, as shown in Table 5-3 to be used in the coupled dynamics analysis [78].

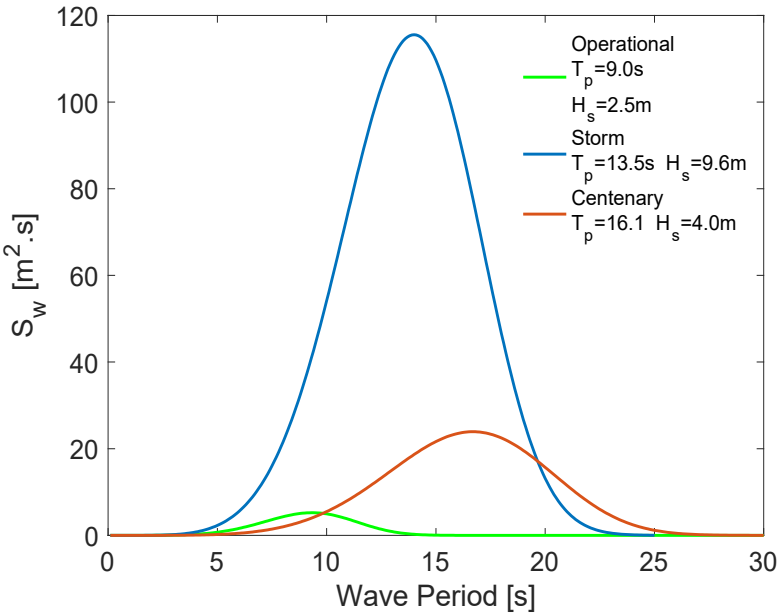

Figure 5-1 Wave Spectrums of Different Conditions on The Japanese Coast

Table 5-3 Wind Conditions

Description	Value
Maximum operational	11.0 m/s
Cut-out	25.0 m/s
Typhoon	41.9 m/s

5.2 Methodology

The structure is proposed in two stages. The first stage was to propose the structure by feasibility study / parametric model.

The structures are proposed based on the parametric study and shortlisted 3 structures and checked the hydrodynamic behaviour. Out of 3 shortlisted structures, one structure was finalized and evaluated that structure for aerodynamic behaviour and coupled with 10 MW wind turbine.

In second stage, three structures were shortlisted based on the optimization through Pareto curve and checked the hydrodynamic and aerodynamic behaviour by WAMIT [79] and OpenFAST [80] respectively. This research methodology is explained in Figure 5-2.

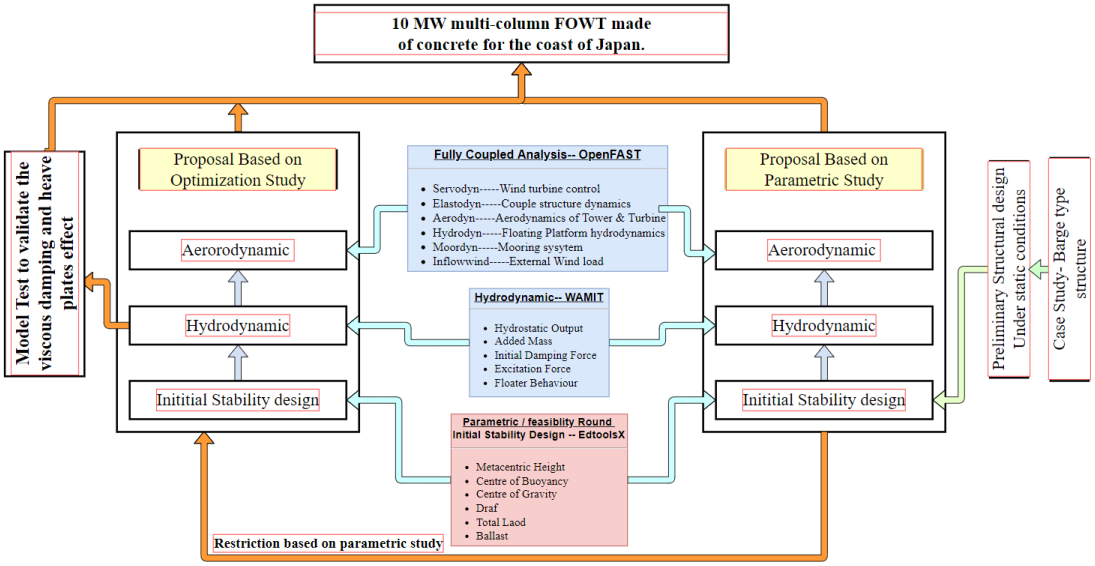

Figure 5-2 An overview of research methodology

5.2.1 Parametric Model

Based on the economical design concept, the main material is consisting of pre-stressed concrete and reinforced concrete resulting in higher displaced volume compared to steel structures. The concrete density of 2,400 kg/m^3 is utilized with compressive strength of 50 MPa.

The precast panel-based concrete structure is adopted considering the advantages of construction work. The concrete semi-submersible floating platform consists of a central hexagonal column with three lower pontoons and three outer pontoons.

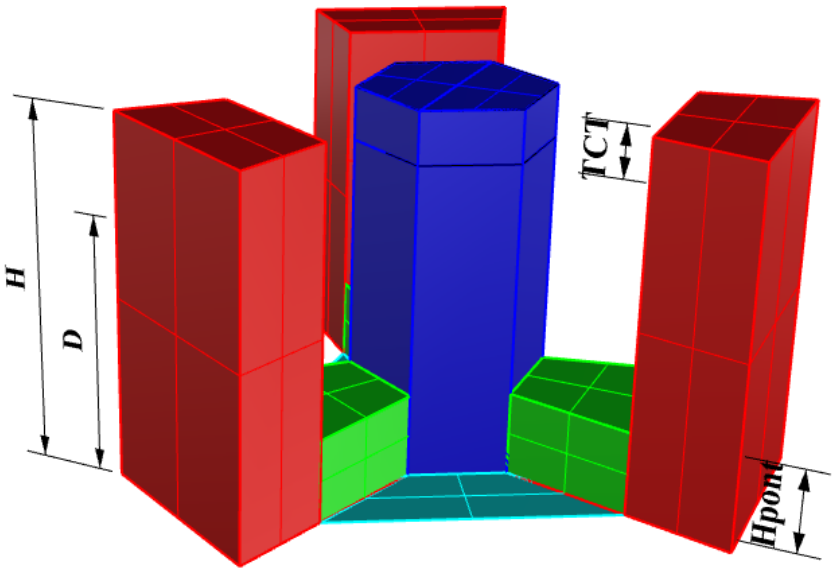

Figure 5-3 Variables of the design. Perspective view of a schematic 3d model.

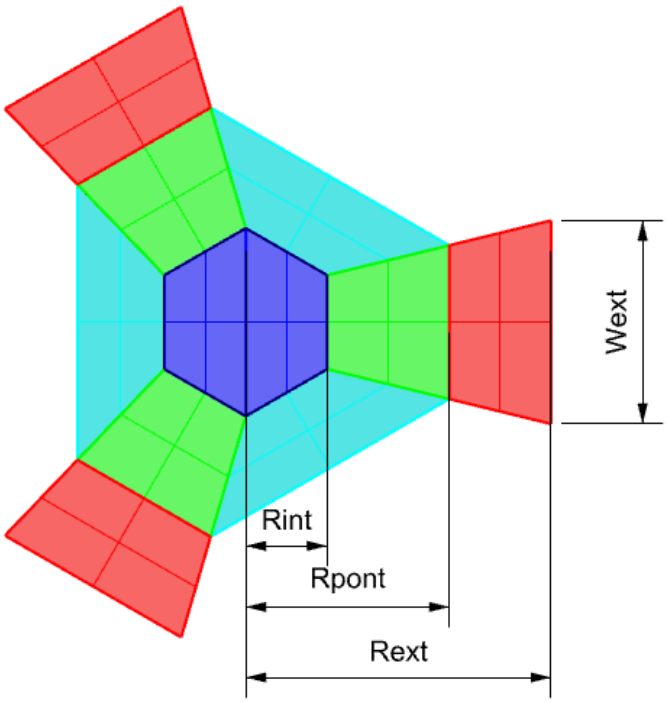

Figure 5-4 Variables of the design. Top view of a schematic 3d model.

On the top of the central hexagonal column, a tower connection thickness, TCT, of a 5 m portion of a solid concrete was assumed to make a stronger connection between steel tower and concrete floater. On the top of the three outer pontoons, the 2 m portion is solid concrete to dissipate the dynamic impact of mooring lines on the concrete floater. A heave plate connecting the pontoons were considered to increase the hydrodynamic damping and added mass levels. The hull and heave plate thickness were considered constant, equal to 0.6 m. Further studies must be done to optimize the hull thickness, as well the heave plate geometry. The geometrical properties are shown in Figure 5-3 and Figure 5-4. The schematic layout of the model is shown in Figure 5-5.

Variables and restrictions were built to achieve feasible solutions. The FOWT is considered feasible if, among the variable space, the alternative satisfies all the proposed restrictions.

5.2.1.1 Variables

A parametric model analysis was built to study the feasibility of the proposed new concrete multi-column floating platform supporting a 10 MW offshore wind turbine.

The variables of the parametric model are shown in Figure 5-4 and Table 5-4. The variables concern the main dimensions of the FOWT.

In the parametric study of the FOWT dimensions, the variables were modified in a chosen range of dimensions as:

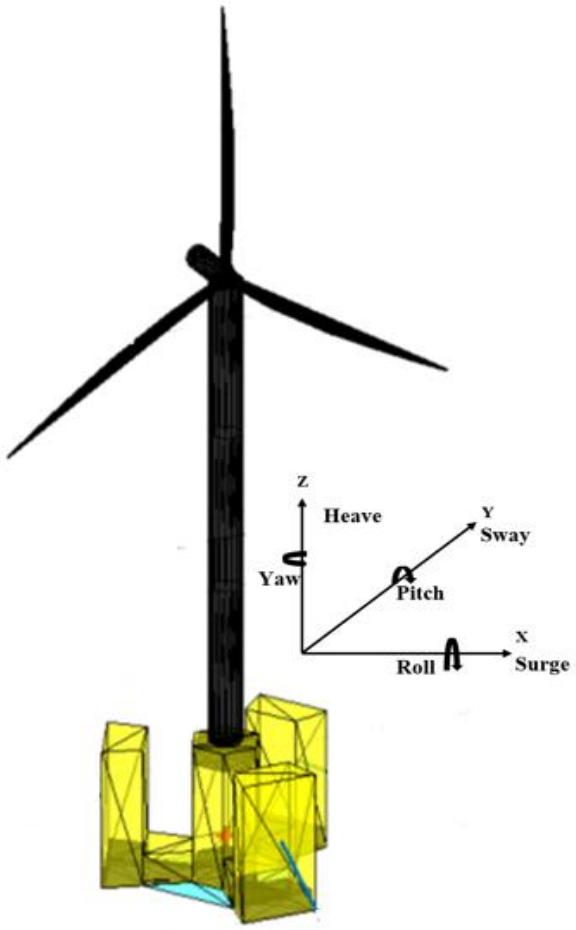

Figure 5-5 Schematic layout of the proposed floater

- External pontoon radius, $Rext$, varied from 22 m to 37 m with an interval of 3 m.
- External pontoon width, $Wext$, varied from 20 m to 32 m with an interval of 2 m.
- Internal radius of outer pontoon, $Rpont$, varied from 20 to 25 m with an interval of 1 m.
- Depth of floating structure, H, varied from 25 m to 40 m with an interval of 3 m.
- Depth of lower pontoon, $Hpont$, varied from 5 m to 10 m.
- The freeboard, $H-D$, is set to 10 m in the fully loaded condition.
- Rint is kept constant, equal to 8 m. As the central column must support the steel tower of 8.3 m diameter for the 10 MW wind turbine, and the need of enough cover depth of concrete for embedding the connection system and proper reinforcement arrangement, $Rint$ equal 8m is the minimum value to support the tower, to avoid excessive vibration and fatigue at the tower base.

5.2.1.2 Restriction

A solution for the new FOWT concrete proposed was considered feasible if it satisfied all the restrictions adopted. The restrictions considered for designing the FOWT concrete are presented as follows.

- Under the loading conditions, the structure is considered safe if the metacentric height GM is greater than 1.0 m.
- The natural heave period of the FOWT must be greater than 15 seconds to prevent the waves highest range of power.
- The natural pitch period must be greater than 20 seconds; for the same reasons presented above, it should be even higher than the natural heave period, so that coupling between the two degrees of freedom are avoided.

Table 5-4 Main dimension and variables considered in the parametric model studies

Parameters / Case ID	SS-01	SS-02	SS-03	SS-04	SS-05	SS-06	SS-07	SS-08	SS-09
Rext [m]	**35.0**	**30.0**	**30.0**	32.0	32.0	28.0	36.0	34.0	37.0
Rint [m]	**8.0**	**8.0**	**8.0**	8.0	8.0	8.0	9.7	8.0	8.0
Wext [m]	**20.0**	**20.0**	**20.0**	26.0	24.0	26.0	22.7	30.0	32.0
Rpont [m]	**20.0**	**20.0**	**20.0**	22.0	22.0	23.0	25.5	25.0	25.0
H [m]	**35.0**	**40.0**	**35.0**	33.0	35.0	31.0	32.2	37.0	40.0
D [m]	**25.0**	**30.0**	**25.0**	23.0	25.0	21.0	22.2	27.0	30.0
Hpont [m]	**5.0**	**5.0**	**8.0**	6.0	6.0	8.0	7.6	8.0	8.0
Hull thickness [m]	**0.6**	**0.6**	**0.6**	0.6	0.6	0.6	0.6	0.6	0.6
Heave plate thickness [m]	**0.6**	**0.6**	**0.6**	0.6	0.6	0.6	0.6	0.6	0.6
TCT [m]	**5.0**	**5.0**	**5.0**	5.0	5.0	5.0	5.0	5.0	5.0

5.3 Intact Stability

In DNV-OS-C301 for the design of water stability and integrity has mentioned the column stabilized floater requirement [81]:

- The area below righting curve should not be less than 30 percent in access to the area below heeling curve for the same angle.
- For all degrees, righting curve should be positive.
- Metacentric height should not be less than 0.3 m.

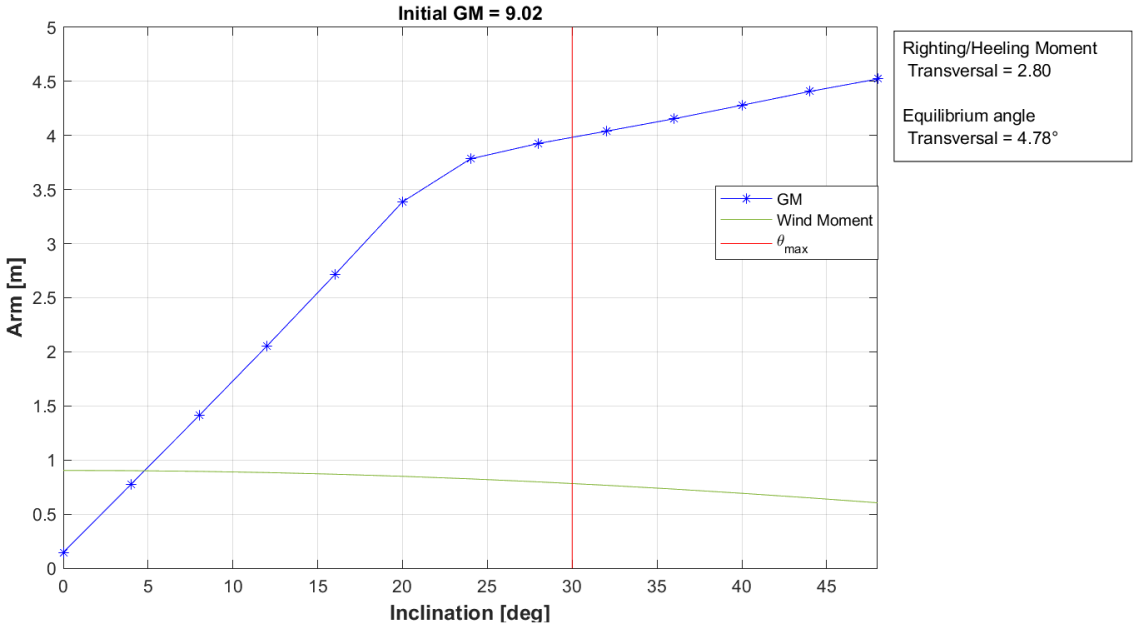

Figure 5-6 intact stability of the structure

The righting curve mainly depends on the restoring capabilities of the column stabilized floating structure while heeling moment mainly depends on effect of wind on the floating structure at some distance far from the rotation centre. It is mentioned that rotation centre is the lowest out of the centre of the lateral resistance of the floating structure. The intact stability of the proposed concrete floating structure of 10 MW wind turbine is shown in Figure 5-6.

5.4 Summary of chapter

The environmental conditions used in this research has been explained. The main geometry of the proposed floater has been presented here with the restrictions and variables used to carry out this research. The feasible cases based on the parametric study have been presented.

- The IEA 10 MW wind turbine was implemented. The cut out wind speed of 25 m/s and average wind speed of 11 m/s have been applied. The rotor has 178.3 m diameter. The blades mass, nacelle mass and tower mass of 143-ton, 639 ton and 539 ton have been taken respectively.
- Three wave conditions operational, storm and centenary and three wind conditions rated, cut out and typhoon have been adopted from ISSC spectrum.
- The water depth in this research has been set to 200 m to evaluate the static, hydrodynamic, aerodynamic and coupled behaviour.
- The metacentric height is 9 m which is higher than the required 0.3 m from the guidelines.

6 Dynamic Evaluation of Concrete Floater based on Parametric Model

In this chapter, hydrodynamic behaviour has been evaluated for the shortlisted cases based on parametric study. The turbine used for these simulations is 10 MW IEA reference wind turbine. The hub height above mean sea level is 129 m with rotor diameter of 178.3 m. The proposed structures are examined under different sea conditions while checking hydrodynamic behaviour in WAMIT and under different wind and wave conditions in checking aerodynamic behaviour in FAST.

6.1 Hydrodynamic Analysis

The stability and motion analysis were performed to confirm the feasibility of the geometry of the concrete semi-submersible floater.

6.1.1 EdtoolsX

The static stability and stiffness matrix of the proposed structure were calculated by using the software EdtoolsX [82]. Also the input files for hydrodynamic analysis were also generated by this tool. The preface of edtools is shown in Figure 6-1.

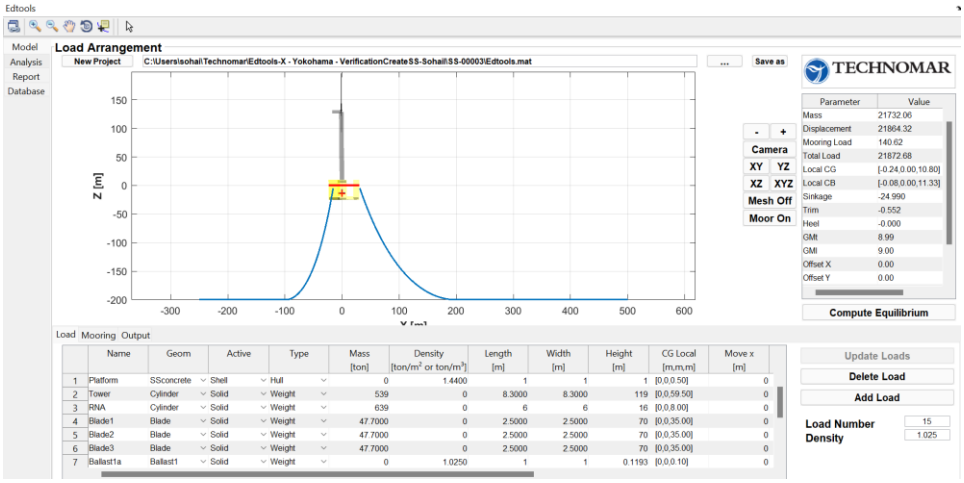

Figure 6-1 EdtoolsX preface

6.1.2 WAMIT

The hydrodynamic behaviour of the FOWT was evaluated first using the WAMIT code. WAMIT uses the potential theory to calculate the hydrodynamic pressure, motions of the body and loads on floating bodies due to the wave incidence in the frequency domain [79].

WAMIT can calculate the following:

- Damping coefficient and added mass of the floating
- Hydrostatic pressure
- Wave exciting force
- Hydrodynamic pressure and effect of flow velocity on the floating body
- Drift force
- Surface pressure

The WAMIT simulation was performed with low order mesh as shown in Figure 6-2.

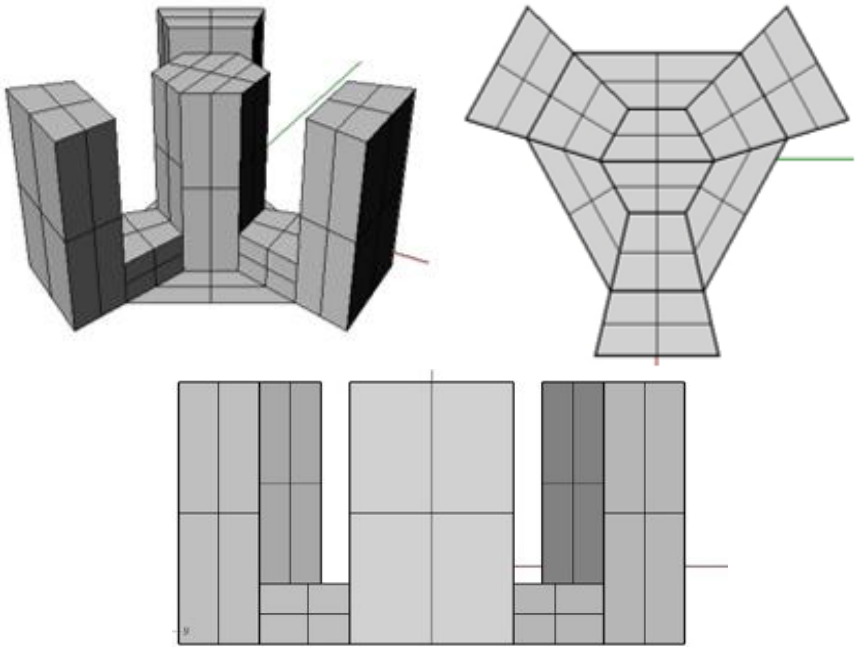

Figure 6-2 Low order mesh considered in the WAMIT code

6.1.3 Added mass, restoring force, Inertial mass, Natural period

In this section, comparison of the three cases have been done based on the added mass, restoring force, inertial mass, natural period displaced volume, centre of gravity and metacentric height in Table 6-1. The heave natural period is the critical one as it should be around 20 sec but for this stage of parametric study, this natural period of heave is considered as sufficient. In this table, added mass as shown in Figure 6-3, restoring force and inertial force is lesser for SS-03 case as the weight or displacement of this case smaller among three cases. This will help us to make our proposal economical.

Table 6-1 Added mass, restoring force, Inertial mass, Natural period

Degree of freedom	Case No.	Added mass	Restoring Force	Inertial mass	Natural period	Displac-ement	CG	GM
		(Ajj)	(Cjj)	(Mjj)	(Tnj) sec	Ton	m	m
Heave (Ton)	SS-01	23114	9935	27303	14	27443	8.65	15
	SS-02	22269	7534	25124	16	25259	10.08	11.15
	SS-03	22375	7534	21732	15	21873	10.8	9
Roll (Ton.m^2)	SS-01	4523310	4038220	30080700	18	27443	8.65	15
	SS-02	4243190	2762880	30090800	22	25259	10.08	11.15
	SS-03	3027810	1932960	25337100	24	21873	10.8	9
Pitch (Ton.m^2)	SS-01	4522740	4038790	30236500	18	27443	8.65	15
	SS-02	4237850	2763620	30240500	22	25259	10.08	11.15
	SS-03	3024470	1933780	25496400	24	21873	10.8	9

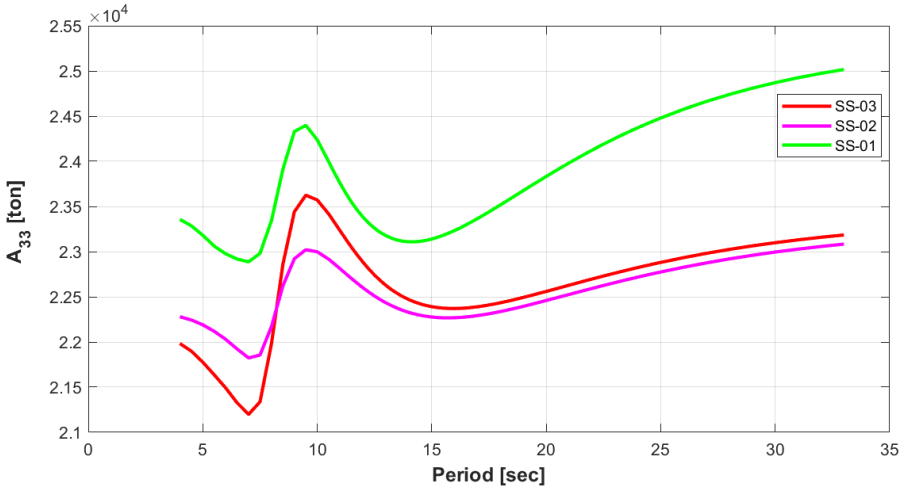

Figure 6-3 Heave added mass comparison

Nine feasible cases were considered in the parametric study which are fulfilling the criteria of hydrostatic stability and natural periods.

Three cases were shortlisted to check the motion behaviour of the structure based on the economy or less weight of the floater.

Table 6-1 presents the results of displacement, GM and natural periods for the cases considered. The cost of the FOWT was considered as a linear function of the displacement. In this case, our merit function was the based on minimizing the displacement of the designed hull.

6.2 Response Amplitude Operators (RAOs)

Response Amplitude Operators are also known as transfer function are taken to check the motion of the structure and its behaviour while floating. RAOs are dependent on the direction of the wave from 0 to 180 degrees. When the wave propagates in the +ve x-axis direction then this is 0-degree wave. In this section RAOs comparison for 3 cases will be discussed for surge, heave and pitch degree of freedom.

6.2.1 Surge

The surge behaviour mostly depends on the mooring configuration. The objective of this research is to not to design mooring lines, but mooring stiffness has been given while calculating the hydrodynamic and aerodynamic calculations. The comparison of the 3 cases has been demonstrated in Figure 6-4. The surge natural period shows good response as for all 3 structures as peak in surge motion is after 20 sec and motions are not high.

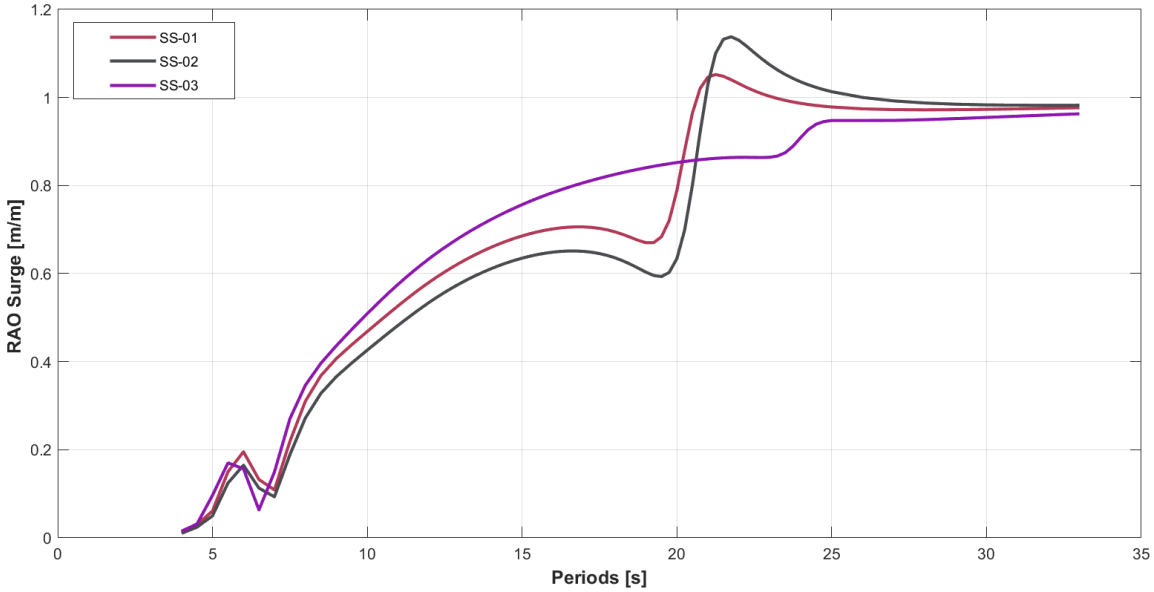

Figure 6-4 Comparison of Surge RAOs

6.2.2 Heave

RAOs heave comparison of 3 cases can be seen in Figure 6-5. Here shape of RAOs for heave just drops before the natural period. This is the special behaviour for semi-submersible floaters as explained Faltinsen [83].

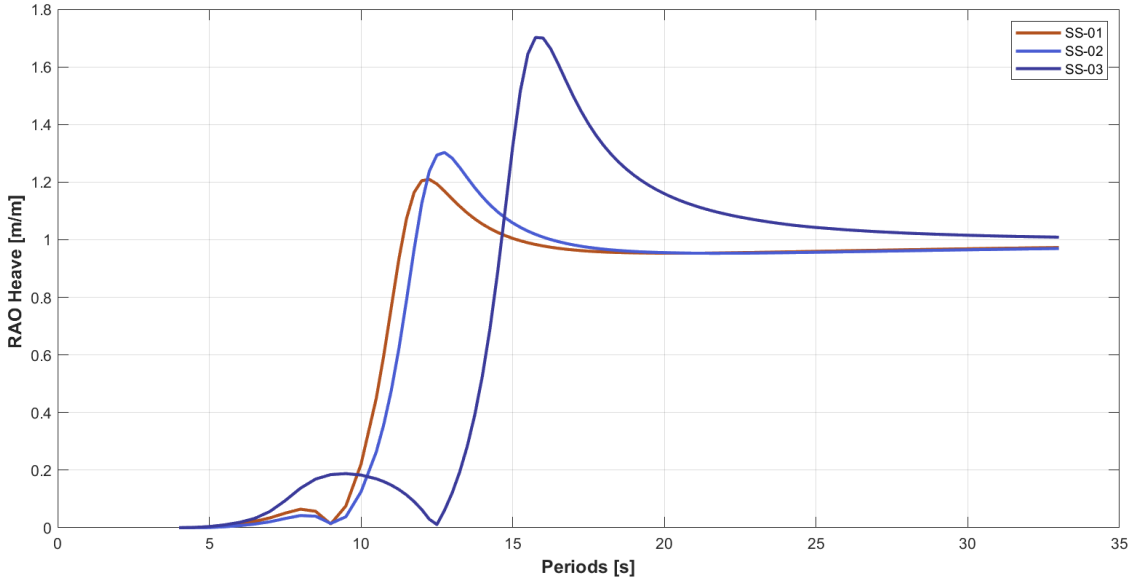

Figure 6-5 Comparison of Heave RAOs

The heave response is not fully drop out, but it just approaches to zero and again rises, the reason due to the availability of the pontoons in semi-submersibles. The sharp difference in between the upper and lower position of the pontoon is the main reason behind this phenomenon.

The maximum heave response is due to the reason when regular waves excite the floater in heave around 1.75 times of the wave amplitude. For larger natural period, response starts converging to 1.0 and longer waves floating structure will move as the amplitude of the waves.

6.2.3 Pitch

The maximum pitch response in Figure 6-6 is for wave heading to the structure at an angle of 0 degree. The other wave heading angle shows lesser response. Out these 3 cases, SS-03 shows lesser response at 4.5 degrees with the natural period of 24.5 sec. The other 2 cases shows relatively higher response of 6.3 degree.

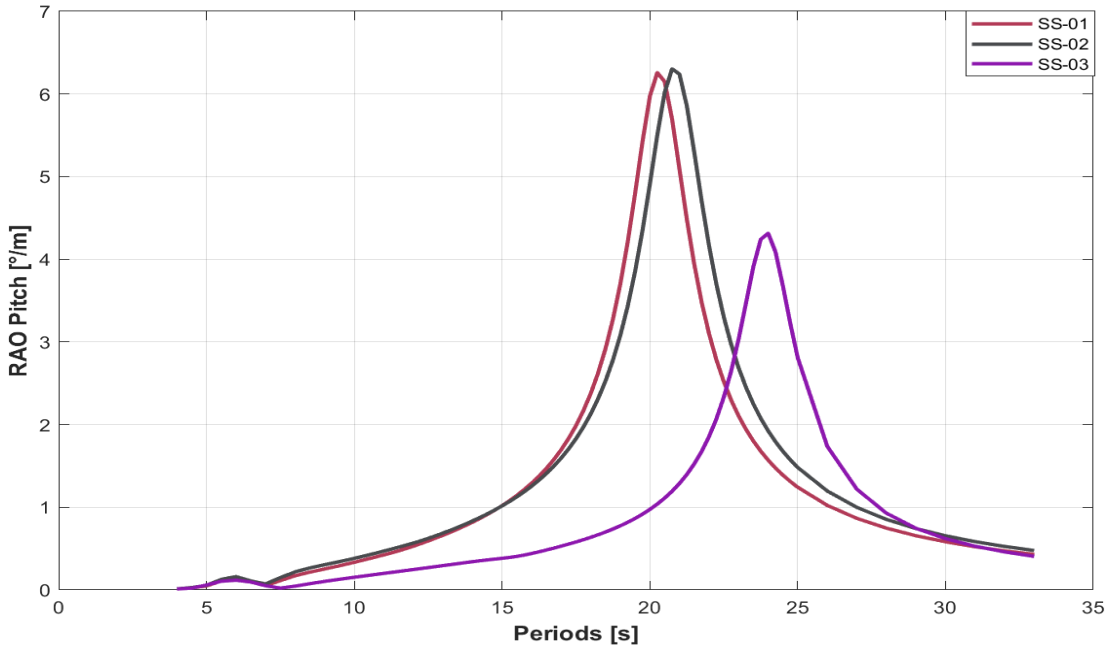

Figure 6-6 Comparison of Pitch RAOs

At a natural period of 6 sec, there is small peak in pitch RAOs, this is due to the excitation of the waves with the structure. The wave length of 6 sec period wave will be:

$$\lambda = \frac{gT^2}{2\pi} \qquad 5\text{-}1$$

$$\lambda = 56\,m$$

This wave length is around the same length of the floater.

It is possible to observe that the SS-03 case had a behavior markedly different from the other 2 cases. This difference was probably due to the smaller displacement.

6.3 Spectral analyses

Spectral analyses were conducted for heave and pitch results obtained from WAMIT. The sea conditions were considered as a wave spectrum, see [84], using the ISSC formulation as:

$$S_w(f) = \frac{A}{f^5}\exp\left(-\frac{B}{f^4}\right) \qquad 5\text{-}2$$

where f is the wave frequency, f_p is the frequency of peak of the wave spectrum and the other parameters can be written as follows.

$$A = 0.1107 H_s^2 \bar{f}^4 \qquad 5\text{-}3$$

$$B = 0.4427 \bar{f}^4 \qquad 5\text{-}4$$

$$\bar{f} = 1.25 f_p \qquad 5\text{-}5$$

The wave spectrum of different conditions on the Japanese coast are shown in Figure 6-7.

The power spectrum of motion response was calculated as:

$$S_{ii}(f) = |RAO_{ii}(f)|^2 S_w(f) \qquad 5\text{-}6$$

where ii is the i-index corresponding to DOF, 33 refers to heave and 55 refers to pitch motion.

The variance of the motion response was estimated from the 0th moment m_0 as:

$$m_0 = \int S_{ii}(f)\, df \qquad 5\text{-}7$$

The significant motion response was computed as $4\sqrt{m_0}$.

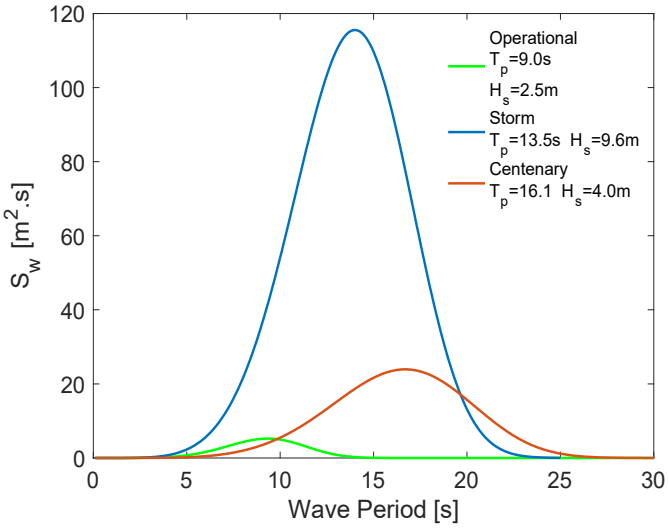

Figure 6-7 Wave spectrums of different conditions on the Japanese coast

The spectral analyses were performed considering the RAO results presented before. The sea conditions utilized the parameters as presented in Table 5-2.

The power spectrum of the response for the three cases for heave and pitch under operational sea state using the ISSC spectrum for waves is shown in Figure 6-8 and Figure 6-9, respectively. The results for storm and centenary conditions followed the same methodology.

The results of spectral analysis are presented in Table 6-2. All the responses were within permissible range. The significant height response for each DOF was calculated and compared for all cases. SS-01 showed higher response values in heave and pitch as compared to the 2 other cases. SS-02 also showed a higher response as compared to SS-

03. In turn, SS-03 showed better response under operational, storm and centenary wave condition mainly for the motion in the vertical plane as heave and pitch.

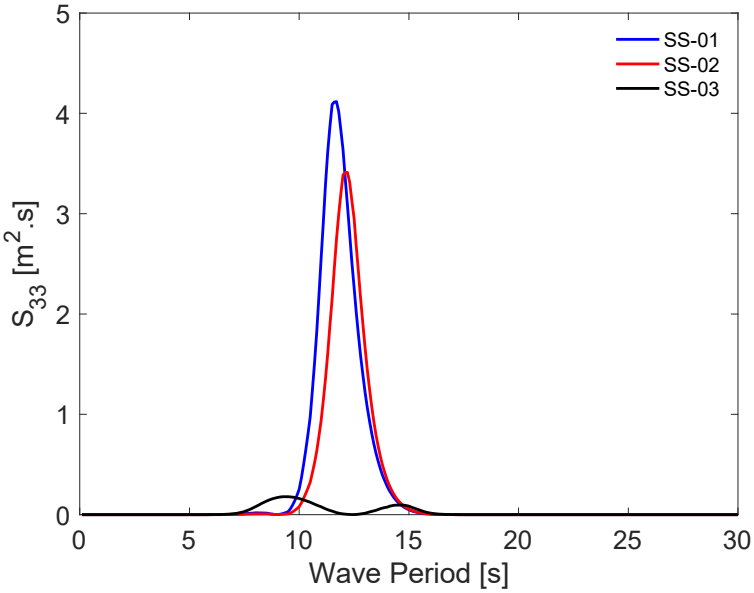

Figure 6-8 Power spectrum of heave motion due to the operational condition

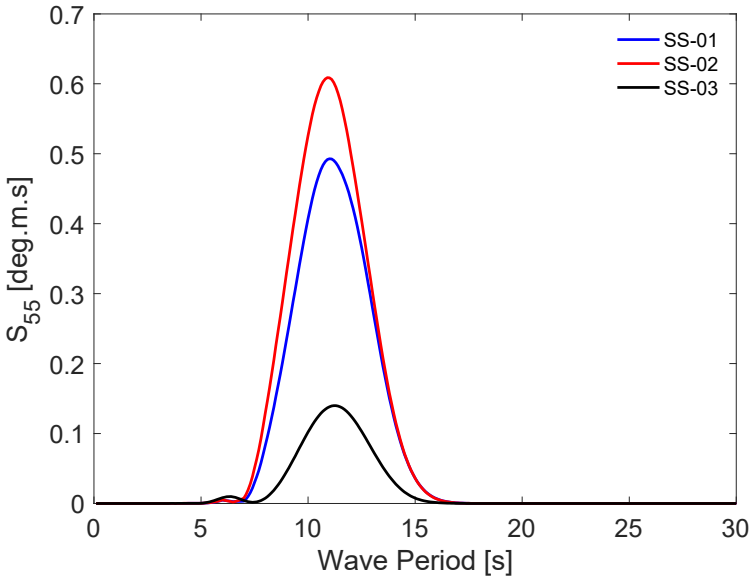

Figure 6-9 Power spectrum of pitch motion due to the operational condition

Surge response was not presented; however, this DOF is greatly impacted by the mooring lines. The mooring lines were not the goal of the present article, and the mooring line design can be a goal for further studies, in which the whole system can be optimized. The SS-03 case was selected as the "potential best hull" because it fulfilled the restrictions adopted and presented the lowest displacement among the three cases compared.

Table 6-2 Significant motion response results of the spectral analysis

Wave Condition	Case ID	Heave Response H_s [m]	Pitch Response H_s [deg]
Operational	SS-01	0.97	0.54
	SS-02	0.84	0.60
	SS-03	0.33	0.27
Storm	SS-01	8.50	8.50
	SS-02	8.72	8.12
	SS-03	6.98	3.60
Centenary	SS-01	3.80	6.70
	SS-02	3.90	6.60
	SS-03	3.90	3.40

6.4 Aerodynamic Analysis

The SS-03 case was used in an OpenFAST analysis to verify the behavior of the FOWT coupled with wind. The wind conditions are presented in Table 5-3.

The fully coupled analysis was performed by OpenFAST [85] by inputting the hydrodynamic properties of the structure evaluated by WAMIT to the HydroDyn submodules, as shown in Figure 6-10.

OpenFAST models the system coupling concerning the environmental conditions (currents, waves and wind) and fully coupled dynamic response (nacelle, rotor, tower, supporting platform and mooring system) under different loading conditions [80].

To validate the OpenFAST model of SS-03, the RAOs from WAMIT were compared with the RAOs from OpenFAST without wind condition. The comparison of RAOs for heave and pitch are shown in Figure 6-11and Figure 6-12, respectively. The difference between WAMIT and OpenFAST is due to the damping values that include the aerodynamics components in OpenFAST. The difference was not large and the RAOs showed a good agreement for this stage of the conceptual design. Further improvements must be included in the next stage.

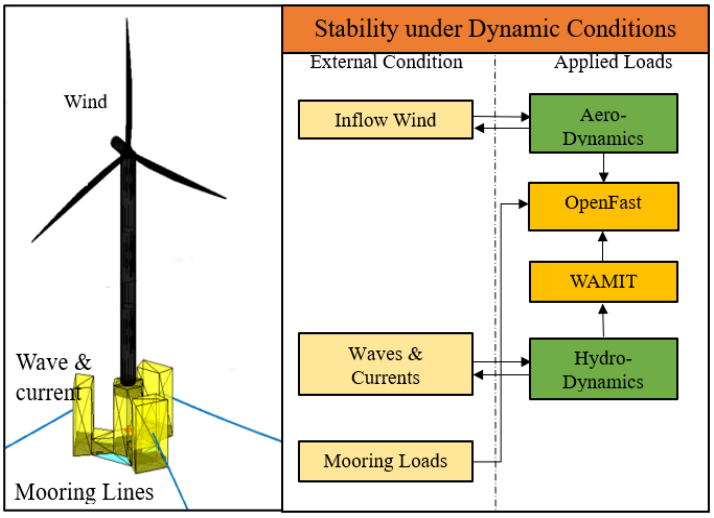

Figure 6-10 The correlation of hydrodynamics and aerodynamics

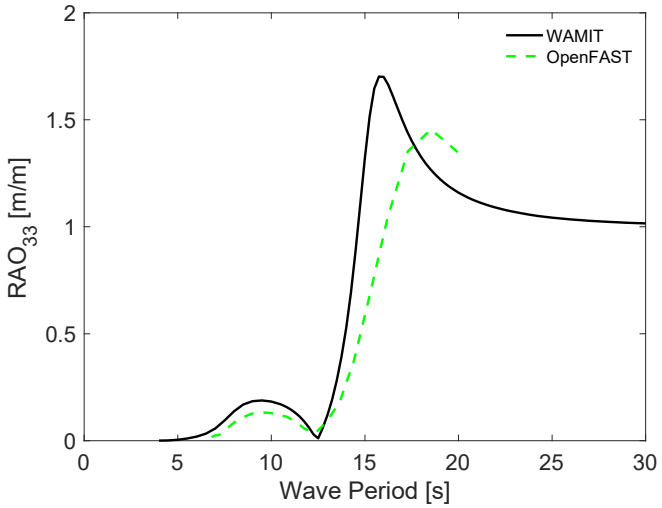

Figure 6-11 Comparison of heave RAOs of WAMIT and OpenFAST calculations

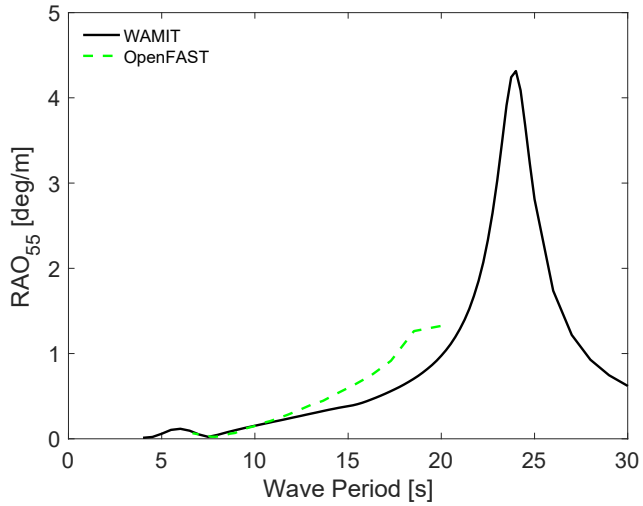

Figure 6-12 Comparison of pitch RAOs of WAMIT and OpenFAST calculations

The motion time series obtained from OpenFAST was utilized to calculate the H_S and H_{max} values for heave and pitch for the combination of environmental conditions, as shown in Table 6-3.

Table 6-3 Coupled dynamics results of OpenFAST analysis

Wave Condition	**Wave Significant Height, H_S**	**Wave Peak Period, T_p**	**Wind Condition**	**Heave H_s [m]**	**Heave H_{max} [m]**	**Pitch H_s [deg]**	**Pitch H_{max} [deg]**
Operational	2.5 m	9.0 s	no wind	0.23	0.38	0.26	0.50
Operational	2.5 m	9.0 s	11 m/s	0.23	0.38	0.33	0.53
Operational	2.5 m	9.0 s	25 m/s	0.23	0.37	0.19	0.37
Storm	9.6 m	13.5 s	41 m/s	3.21	4.34	3.80	5.06
Centenary	4.0 m	16.1 s	11 m/s	2.66	3.58	1.65	2.05

The proposed FOWT showed good response in operational wave condition with no wind, rated wind and cut-out wind speed. The platform also showed appropriate results for storm wave with 41 m/s wind and centenary wave with rated wind speed.

For all DOF, the ratio between the motion high significant response and significant height of the wave was lower than 1, which represented that the FOWT worked well to reduce the wave energy. For operational condition, for example, the decrease of heave motion was around 80%.

In summary, the main properties of the "best potential case" can be shown in Table 6-4. Detailed geometry can be described as follows and some considerations are presented.

Table 6-4 Main properties of the proposed concrete FOWT

Parameter	Value
Displacement	21,873 ton
CG	10.8 m
CB	11.3 m
D	25.2 m
GM	9.0
H	35.0 m

The distance from the central hexagonal column to the lower pontoons and outer pontoons are 14 m and 25 m, respectively. The side of the hexagon is 9 m wide, lower pontoons are 15 m wide, and outer pontoons are 20 m wide. The lower pontoons depth is 8 m while the outer pontoon depth is 35 m, the same as the floater depth. The heave plates are also mounted in between lower pontoons. The wall and slab thicknesses are taken as 0.6 m. The overall weight of the platform is 20,411tons, including ballast.

A standard seawater ballast system approach was adopted to reduce the cost as well as to ease the transportation and installation. Seawater of density 1,025 kg/m3 was taken as ballast. Ballast was arranged in different pontoons to adjust the stability and to achieve the required draft of the concrete semi-submersible floater. The total ballast weight is 3,692 tons.

6.5 Mooring Tension

To reduce the floating platform motions, the restoring force to counter the environmental loadings has been provided through the mooring lines. Here in this research catenary type mooring line have been used. In catenary mooring lines, part of lines has been rested on the ocean bed. When the wave load is applied on the structure, the restoring force against that load is generated. As the water depth increases the weight of the mooring line increases and the vertical force from the mooring lines to the floating platform is also increased.

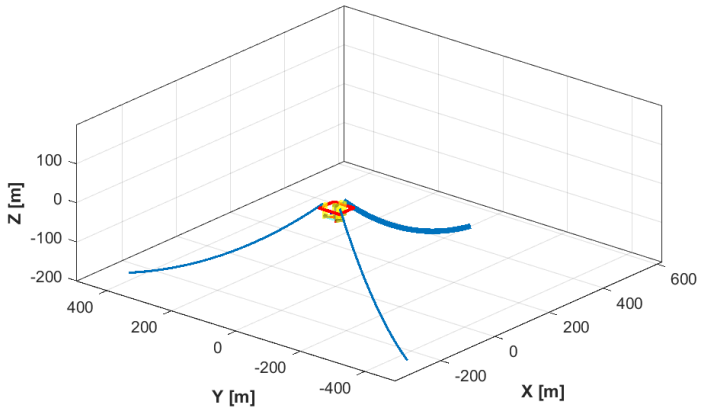

Figure 6-13 Mooring line arrangement

In this research the water depth used is 200 m which is comparatively higher than normal floating structure. The mooring line arrangement can be seen in Figure 6-13. The maximum tension forces are

Line 1 : 7268 KN

Line 2 : 1315 KN

Line 3 : 1315 KN

These are the forces when wind turbine is operating under operational sea conditions with rated wind speed of 11 m/s. As the surge motions in this case is at 11 m can be seen in Figure 6-14. So, the mooring tension have been checked at 11 m of surge condition.

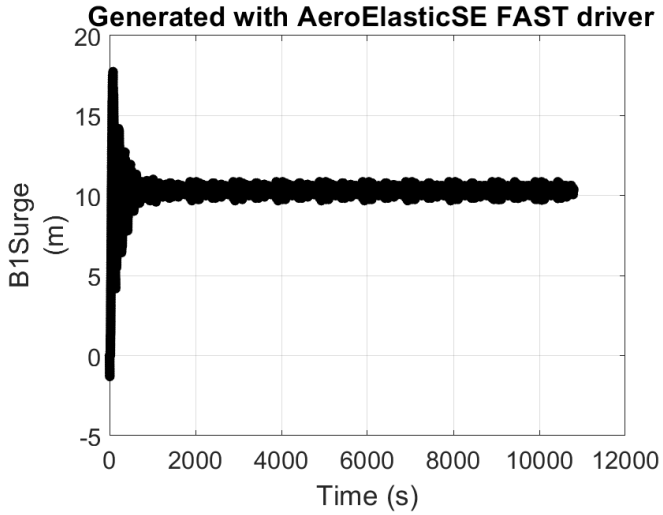

Figure 6-14 Surge motions for Operational Sea states with rated wind speed

Although this mooring tension is big but as compared to the cable stayed bridge, this is not so large. In Toyota Arrows Bridge as shown in Figure 6-15, which is located in between Tomei expressway and Tokai expressway, the bridge is a 4-span continuous PC / steel composite cable-stayed bridge, with a bridge length of 820 m (maximum span: 235 m) and a total width of 43.8 m with an integrated upper- and lower-line structure (8 lanes). It is one of the largest bridges on the road and the largest span in the world as a cable-stayed web bridge [86].

Figure 6-15 Toyota Arrows Bridge completed photo [90]

Since this bridge is a one-sided cable-stayed bridge with a total width of 43.8 m, a maximum tension of about 20000 KN acts on the cable-stayed cable anchorage on the main girder side when the design load is applied (one anchorage).

In comparison to this cable stayed bridge, which is functional since 2006, the tension force is lesser and can be accommodated with care.

6.6 Summary of chapter

- Based on hydrodynamic behavior, SS-03 has been finalized on the less displacement or less weight of the floater.
- SS-03 has lesser added mass, restoring force and inertial mass as compared to the other cases. This is due to the fact this case was finalized based on less weight.
- The natural heave period is 15 sec, which is smaller and will be modified in the next round of optimization study. The heave motions are not fully zero, but it just near to zero around 8 sec and again rises, the reason due to the availability of the pontoons in semi-submersibles. The abrupt difference in the upper and lower pontoon position was the major cause of this phenomenon.
- At 6 sec natural period, pitch RAOs has a small peak, the reason is structure was synchronized with the excitation of the waves. The wavelength will be 56 m for of a 6 sec period wave.
- The significant height response was calculated and compared for 3 cases. SS-01 had bigger response values in pitch and heave in comparison to other cases. SS-02 also had a larger response value than SS-03. On the other hand, SS-03 had good response for storm, centenary and operational wave condition.
- RAOs had a good agreement for current level. There is a small difference between OpenFAST and WAMIT and this is due to the difference in damping values that is different for aerodynamics components.
- The proposed floater had good reaction under operational wave condition with rated wind, no wind and cut-out wind speed. The floater also had good results for storm wave c conditions with 41 m/s wind and centenary wave conditions with rated wind speed.

- For the water depth of 200 m, the maximum mooring tension in 1 mooring line is 7268 KN.
- The final was selected as it has lower coupled motion response and the lower displacement under various environmental conditions.

7 Model Test

In this chapter, model test of the shortlisted case has been explained in the wave tank. The 1:60 scale were conducted to evaluate the hydrodynamic response of the proposed structure under different heave plates position. The structure response was checked under regular waves, irregular waves and transient waves. The free decay test for different heave plate position have been explained.

The model test case has been shortlisted based on the restrictions already explained in Chapter 5. These restrictions are :

- Metacentric height should be greater than 1.0.
- Heave natural period of the floater must be greater than 20.0 sec.
- Pitch natural period of the floater must be greater than 23 sec.
- Tilt angle must be less than 7 degrees.

Based on these conditions, SS-07 case has been shortlisted for model test as shown in Table 7-1. As this case is fulfilling the requirements as well as restoring moment is also in appropriate range.

Table 7-1 Selection of the case for Model test

Case ID	Mass [ton]	CG [m]	GM [m]	Heave Natural Period [s]	Pitch Natural Period [s]	Restoring Moment [ton-m]
SS-01	27303	8.65	15.00	14.4	18.0	35739
SS-02	25124	10.08	11.15	16.0	22.0	24446
SS-03	21732	10.80	9.00	15.0	24.0	17068
SS-04	24653	9.28	12.30	16.7	20.0	26462
SS-05	25126	9.38	12.00	16.0	20.0	26311
SS-06	20810	10.59	6.19	21.0	29.0	11241
SS-07	27142	13.83	8.23	19.5	23.0	19493
SS-08	32432	7.54	14.76	19.0	19.0	41773
SS-09	43549	5.92	19.70	18.0	16.0	74866

7.1 Experimental setup

7.1.1 Scaled model

A reduced scaled model has been constructed which was similar to the prototype at a scale of 1:60 to check the proposed floater response under waves. The original model dimensions are shown in Figure 7-1 and Table 7-2. The scale model is shown in Figure 7-2.

Table 7-2 Main dimension and variables for the case used in model test

	Dimensions [m]
Rext:	36.0
Rint:	9.7
Wext:	22.7
Rpont:	25.5
Draft:	22.2
Depth:	32.2
Hpont:	7.6
Hhp:	5.3
Hull thickness:	0.6
HP thickness:	0.6
Tower Connection Thickness:	5.0

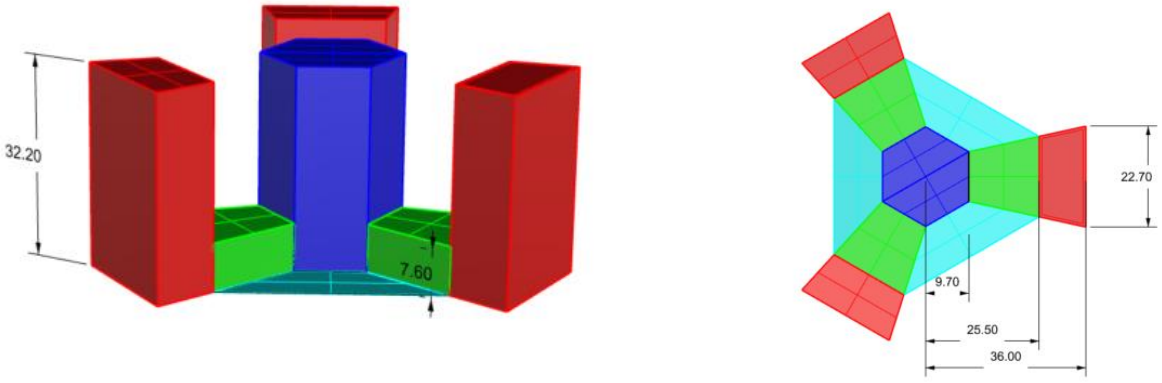

Figure 7-1 Full scale model dimensions used in the experiment

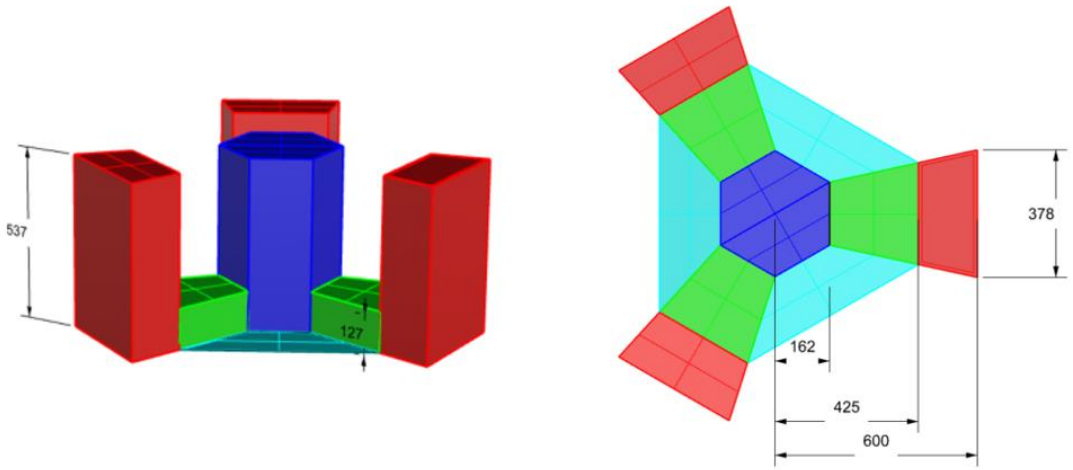

Figure 7-2 Model dimensions used in the experiment at the scale of 1:60

The experiments were conducted at the towing tank of the University of Tokyo, Japan. The length of towing tank is 85 m, width is 3.5 m and depth are 2.4 m as shown in Figure 7-3. The floating model was placed 50 m away from the wave generator setup.

Acrylic made deck was installed to attach the spring mooring lines and keep the targets in position which was utilized for motion capturing tools. Six degree of freedom (6DOF) floater motions have been computed using Qualisys® which is an optical motion capturing system. It consists of four cameras and 6 targets which are attached on the surface of model deck.

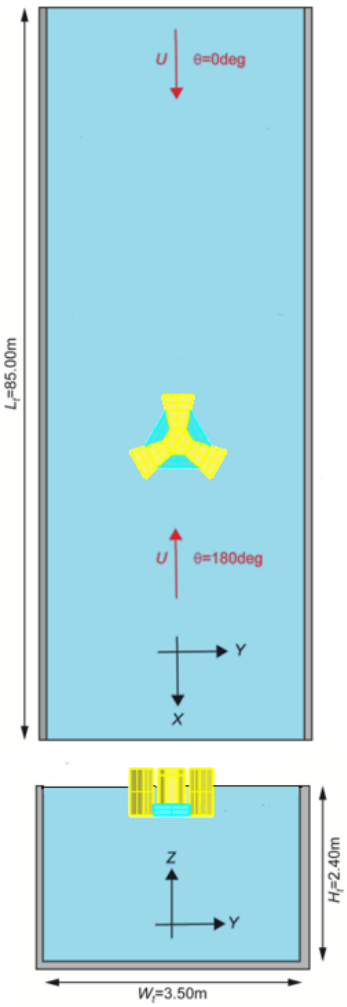

Figure 7-3 Towing tank dimensions

7.1.2 Wave conditions

The irregular and regular wave conditions in full scale which was carried out during the model test are presented in

Table 7-3 and Table 7-4.

Table 7-3 Irregular wave conditions in full scale

Condition	Wave Significant Height, H_S	Wave Peak Period, T_p
Operational	2.5 m (4.17 cm)	9.0 s (1.16 s)
Storm	6.0 m (10 cm)	13.5 s (1.74 s)
Centenary	3.4 m (5.56 cm)	16.1 s (2.08 s)

7.1.3 Model test conditions

The experiment was done on three different models. The type of models was based on the heave plates orientation as mentioned in Figure 7-4. In part a, there is no heave plates between the lower pontoons. In part b, only horizontal heave plates have been installed between the lower pontoons. In part c, both horizontal as well as vertical heave plates have been installed between the lower pontoons.

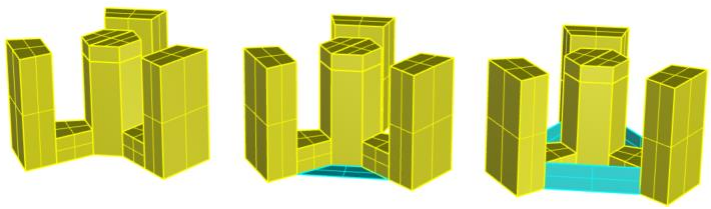

(a) (b) (c)

Figure 7-4 Types of models based on heave plates orientation

Table 7-4 Regular wave conditions in full scale

Condition	Regular Wave Height, H_S	Range of Wave Period, T_p
A	1.0 m (1.67 cm)	5.0 s (0.65 s)
B	1.0 m (1.67 cm)	10.0 s (1.29 s)
C	0.87 m (1.45 cm)	15.0 s (1.94 s)
D	0.87m, 1.75m, 3.5m (1.45cm, 2.90 cm, 5.81 cm)	17.0 s (2.19 s)
E	0.87m, 1.75m, 3.5m (1.45cm, 2.90 cm, 5.81 cm)	20.0 s (2.58 s)
F	0.87m, 1.75m, 3.5m (1.45cm, 2.90 cm, 5.81 cm)	25.0 s (3.23 s)
G	0.87m, 1.75m, 3.5m (1.45cm, 2.90 cm, 5.81 cm)	30.0 s (3.87 s)

7.2 Data Analysis

For data analysis, full heave plate case has been shortlisted to check behaviour of floater against the operational sea stats which has significant wave height of 2.5 m and peak wave period of 9.0 sec. This operational wave has most of the energy in between 0.5 Hz to 2.5 Hz can be seen in Figure 7-5

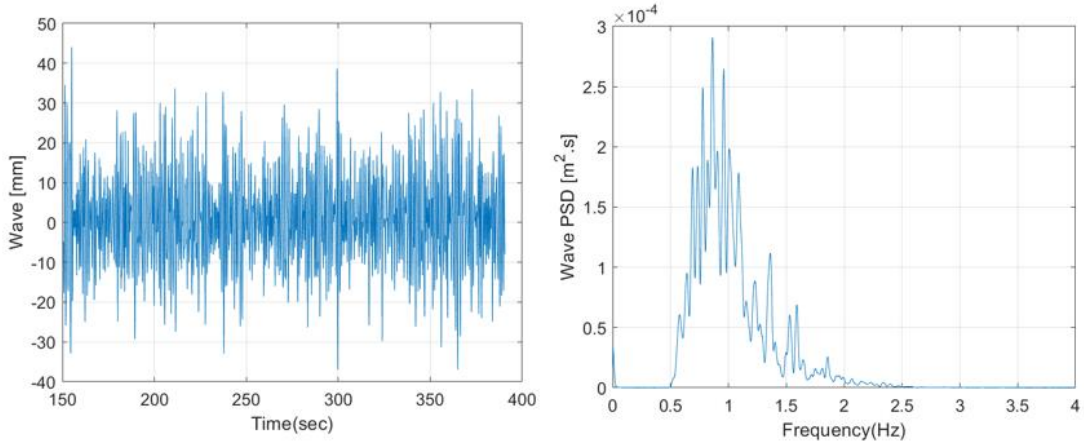

Figure 7-5 Wave Signal and Spectral Response of the Floater

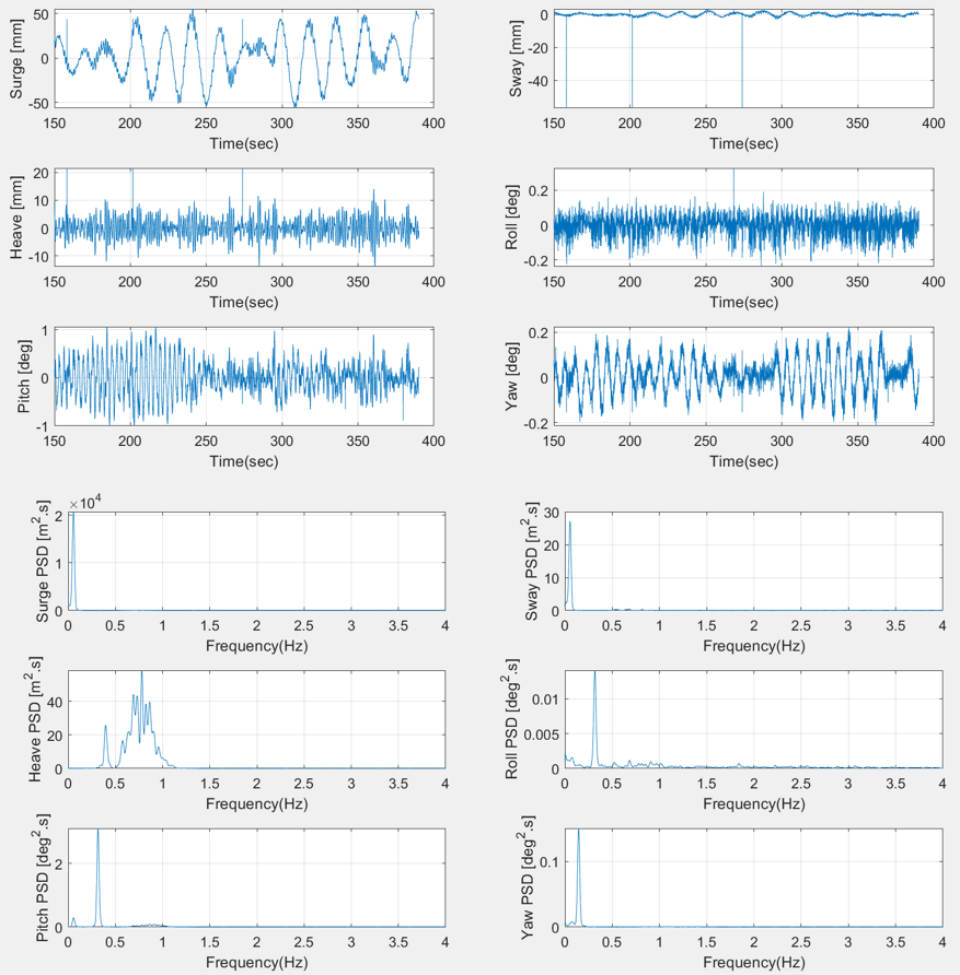

Figure 7-6 Motion Signal and Spectral Response of the Floater

The signal for both wave response and motion response have been cut from 150 sec to 390 sec to check the spectral response for the same range of signal as shown in Figure 7-5 and Figure 7-6. All 6 DOF (surge, sway, heave, roll, pitch and yaw) time series and spectral density has been presented in Figure 7-6.

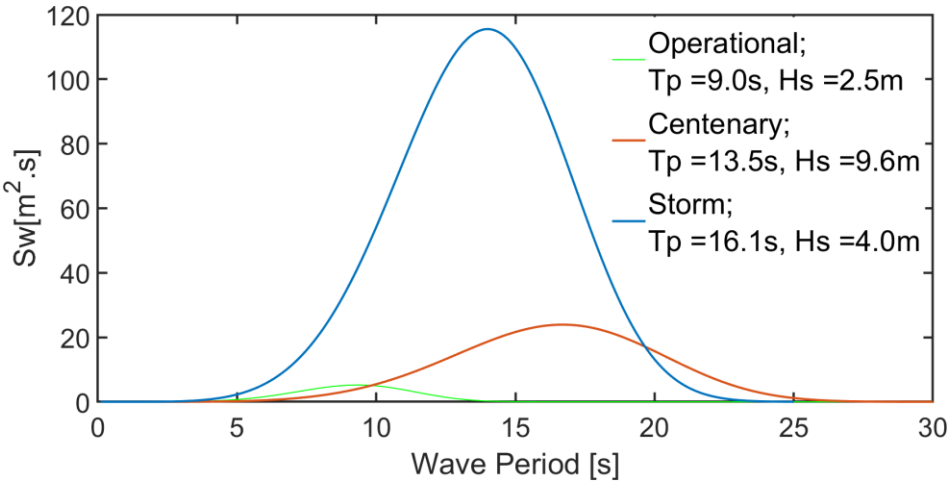

Figure 7-7 Wave Spectrums of Different Conditions on The Japanese Coast

In Figure 7-7, wave spectrum of different sea conditions has been presented for the coast of Japan. As only operational case has been verified in this data analysis, so from here we can observe that the operational wave has the energy in between 5 sec to 13 sec. So in this section the experimental data also checked in this range. The RAOs for Irregular conditions have been calculated by using following equation:

$$RAO(\omega) = \left(\frac{S_{Resp}(\omega)}{S_{\omega ave}(\omega)}\right)^{0.5}$$

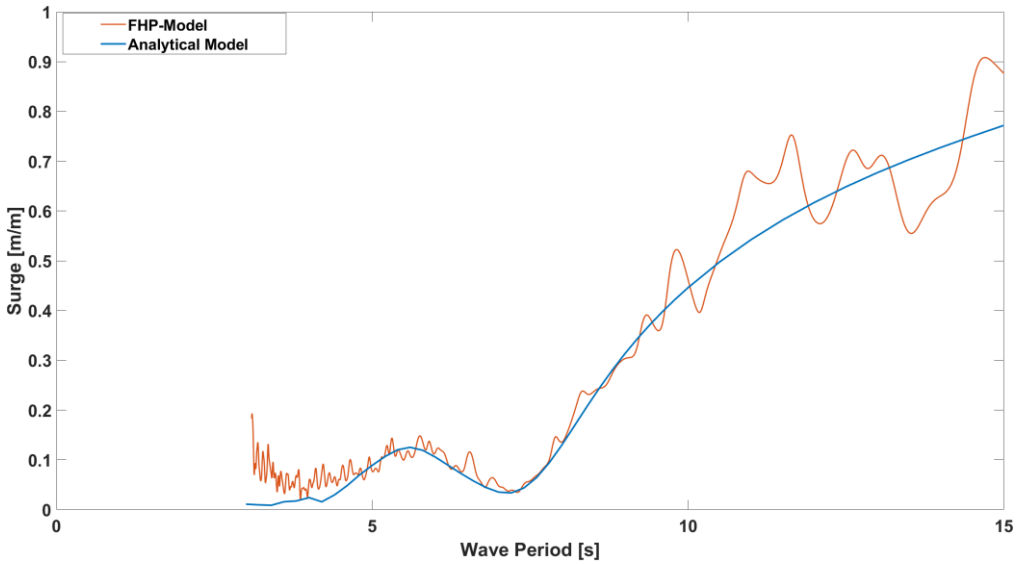

Figure 7-8 Comparison of RAOs between Experiment and Analysis for Surge

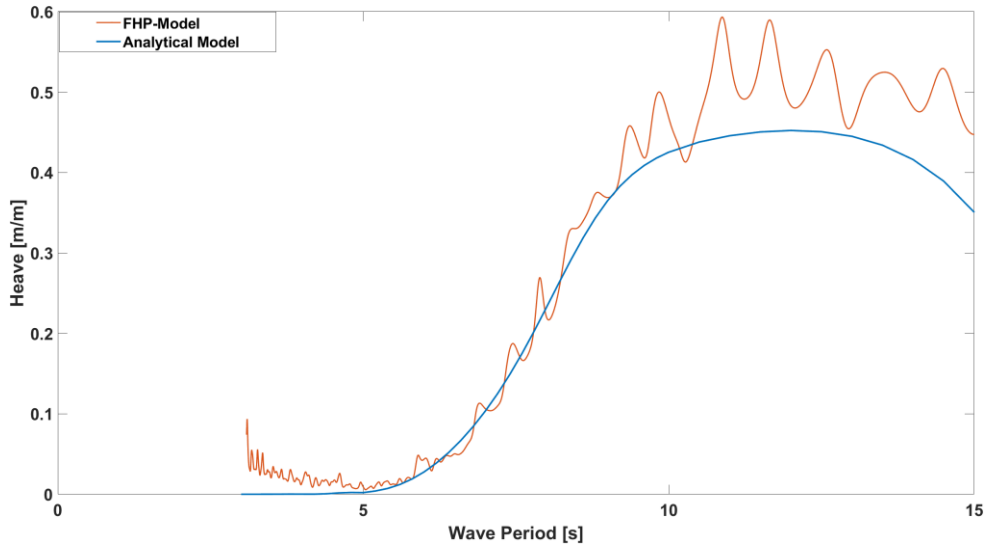

Figure 7-9 Comparison of RAOs between Experiment and Analysis for Heave

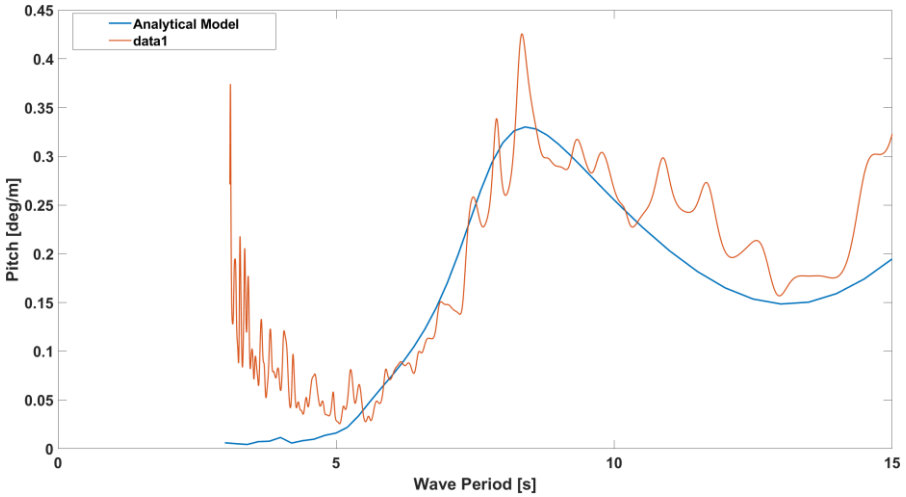

Figure 7-10 Comparison of RAOs between Experiment and Analysis for Pitch

The comparison of surge, heave and pitch transfer function between model test and analysis have been presented in Figure 7-8, Figure 7-9 and Figure 7-10. This comparison has been done for operational wave conditions in between 5 sec to 13 sec.

7.3 Comparison of Heave Plate behavior under Operational and Storm Conditions

7.3.1 Heave Comparison

In this section, RAOs comparison of 3 different models i.e. full heave plate model, middle heave plate model and without heave plate model have been done under operational sea conditions and storm sea conditions.

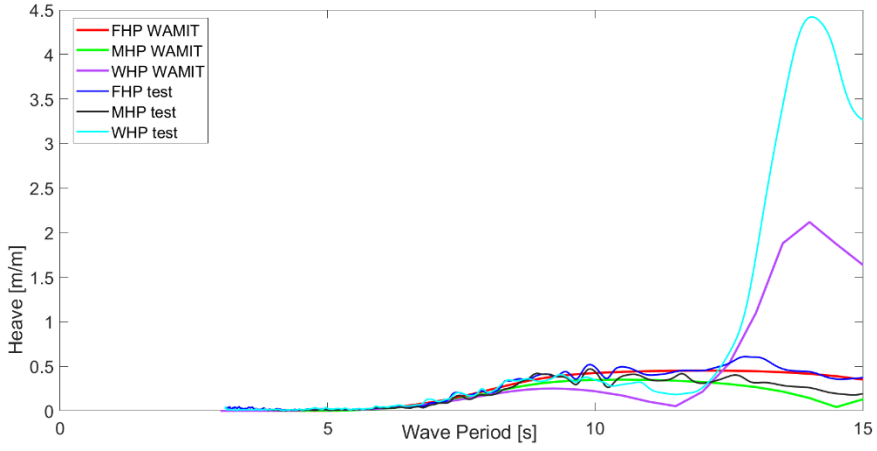

Figure 7-11 RAOs Heave Comparison for Operational conditions

Figure 7-11, Heave RAOs comparison have been done under operational conditions. In this figure WAMIT results for full heave plate (FHP), middle heave plate (MHP) and without heave plate (WHP) have been compared with the respective model test results. The is good agreement between model teat results and WAMIT results for FHP and MHP but there is a difference in between simulation and model test results for WHP. The period is same for both simulation and model test but motions in model test are larger. When there is no heave plates in between lower pontoons, waves starts galloping in

vertical direction so in experiment without heave plates, motions are higher as WAMIT couldn't simulate very well this behaviour. Under operational conditions, proposed model with any of FHP, MHP and WHP is fulfilling the requirements.

In Figure 7-12, comparison of heave RAOs under storm conditions have been done. Here, there is good agreement between simulation and model test for all the cases. But for here, period is different for FHP, MHP and WHP. The period for WHP is 14 sec and this period is in between the ocean waves period of 5sec to 20sec. On the other hand, both for MHP and FHP, the period is beyond 20 sec. So, the model with middle heave plates is suitable for storm conditions.

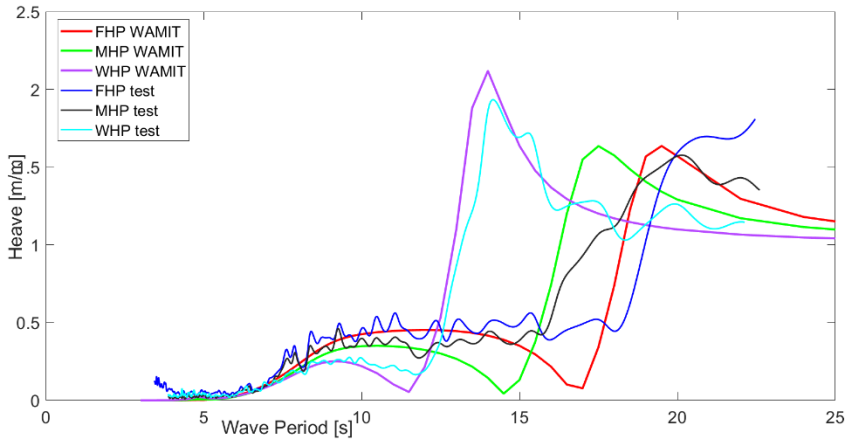

Figure 7-12 RAOs Heave Comparison for Storm conditions

7.3.2 Pitch Comparison

In this section, pitch motion under operational and storm conditions have been presented in Figure 7-13 and Figure 7-14. Under operational conditions, pitch motions for all the cases are less than 0.5 degrees and under storm condition, pitch motions are less than 2 degrees for the period of 20 sec.

From pitch motions comparison, model with MHP is suitable based on the period and motions.

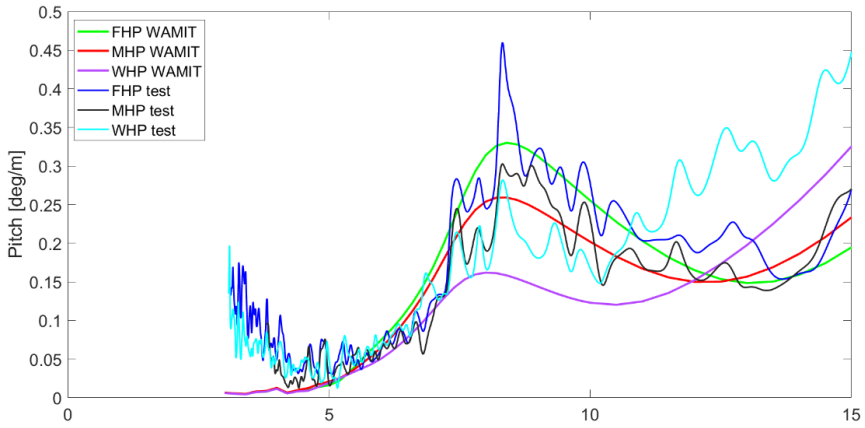

Figure 7-13 RAOs Pitch Comparison for Operational Conditions

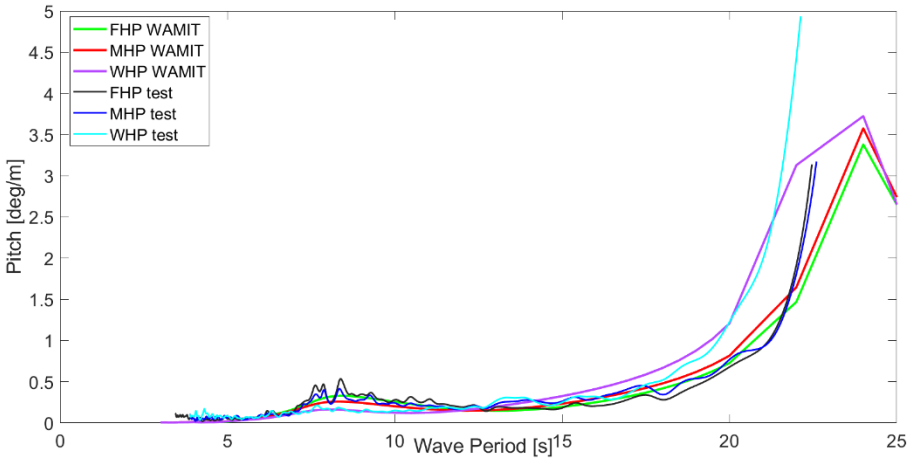

Figure 7-14 RAOs Pitch Comparison for Storm Conditions

7.3.3 Surge Comparison

Surge motions and period are also within permissible limit under storm and operational conditions for all the cases as shown in Figure 7-15 and Figure 7-16.

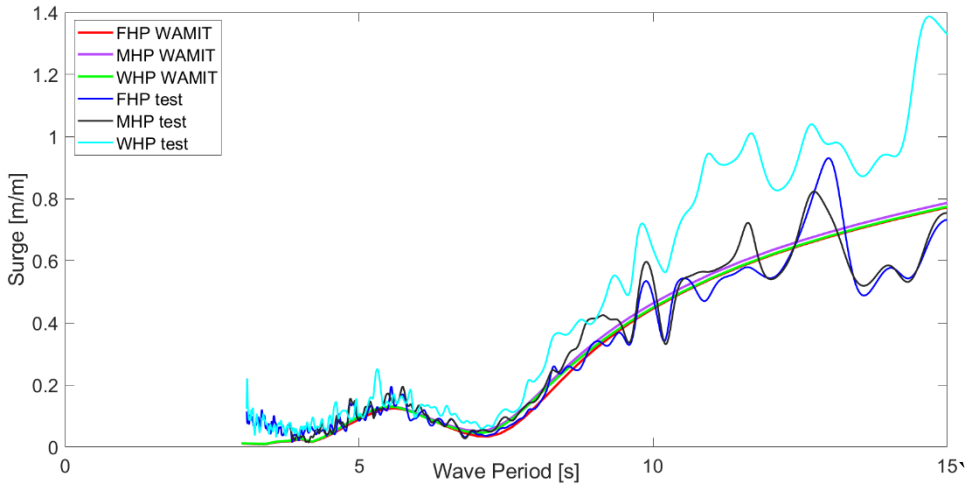

Figure 7-15 RAOs Surge Comparison for Operational Conditions

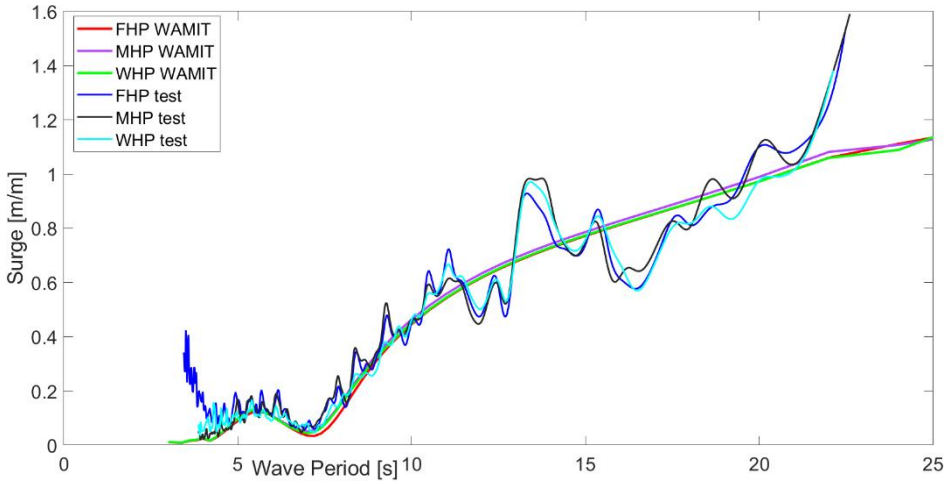

Figure 7-16 RAOs Surge Comparison for Storm Conditions

7.4 Summary of chapter

- The case for model test has been finalized based on the restrictions which heave and pitch natural period, metacentric height and tilt angle.
- The 3 different model tests have been done to check the effect of heave plate on floater response and to check the floater natural period is either inside the wave period range or away from that.
- Upon comparison, middle heave plate (MHP) has been finalised based on the evaluation of model test and simulations results. As MHP is accomplishing the conditions for operational and storm sea states.

8 Conclusions

Floating offshore wind turbine has been developed in last decades especially in Europe. Now the researchers are focussing on proposing the support structures made up of concrete other than steel. The reasons are reduced carbon emission, reduced cost and quite common construction skills for concrete structures.

Therefore, this study aims to propose a concrete multi-column floater for 10 MW floating offshore wind turbine. The mooring connection fatigue behaviour and structure stresses of the barge floating structure has been evaluated by the finite element tool COM3. The structure has been proposed in 3 rounds. The geometric and structural design of the 1st proposal has been done based on the static loading. The 2nd proposal has been presented based on parametric study. The behaviour in waves of the structure was confirmed by numerical calculations using WAMIT and OpenFAST codes. At the end model test has been done to validate the added mass, damping and hydrodynamic calculations.

8.1 Summary of the Chapters

Following conclusion have been drawn from this research:

- In 1st round under static load conditions, 5 m tower connection thickness was considered to compensate the 10 MW WTG loadings and vibrations.
- 50 cm slab thickness is decided which is larger than necessary slab thickness. The concrete cover is considered as 70 mm. Minimum area of steel governed due to larger concrete section.
- The minimum required thickness of wall for shear is 270 mm.
- Out of 700 mm wall thickness, 160 mm is compression one and rest is tension zone. To accommodate the applied hydrostatic loads, minimum 100 mm compression zone is required as per DNVGL guidelines.
- In 2nd stage, after assessing hydrodynamic analysis, SS-03 demonstrates good response in pitch and heave for different wave. In the coupled aerodynamic analysis, SS-03 also demonstrates good response for various groupings of wind conditions and sea states.
- The final floater was selected based on the smallest displacement and smallest significant heigh motion response under the environmental conditions considered.
- In 3rd stage, proposed concrete floater model test for 10 MW wind turbine was finalized based on the Restoring moment and restrictions of heave and pitch natural period.
- In hydrodynamic behaver evaluation, SS-07 demonstrate better response in heave and pitch as compared to the other shortlisted cases. In coupled aerodynamic evaluation, SS-07 showed the better response under different sea conditions and wind conditions.

8.2 Conclusions

- Depth of lower pontoons, H_{pont}, found to be critical. By increasing the depth of lower pontoons, the natural period of the proposed floater increased.
- Depth to width ratio should be 0.5.

- Middle heave plate (MHP) has been proposed based on the comparison of simulations and model test results. As MHP is fulfilling the requirements for operational and storm sea conditions.
- According to ACI 224.1R-07, the crack width is 0.129 mm. In DNVGL, crack width opening for splash zone is 0.2 mm which is greater than calculated crack width.

Based on the objective of this research, the final conclusion is the proposed structure shows good response and fulfilled the restrictions adopted during this research. The structure is good under hydrodynamic and aerodynamic loadings and can be utilized for structural design for future research.

8.3 Future Recommendations

Following future recommendations have been proposed for this research:

- It was presented that the data analysis for the model test are undergoing to validate the hydrodynamic responses as well as to calculate the corrected added mass and damping. It is necessary to validate the model test results with the reduced scale model with corrected added mass and damping.
- From the model test after verification of heave plates behaviour, it is necessary to finalize the proposal based on heave plates configurations.
- It is necessary to propose the Connection design (Tower to floater connection and Fairleads connection) and concrete structural design.
- The behaviour of the proposed floater under coupled dynamic loadings by using Finite Element tool is compulsory to check the durability of concrete structure and Fatigue performance.

9 References

[1] 2018, “Wind Europe. Offshore Wind in Europe. Key Trends and Statistics 2017. Wind Europe.”

[2] IRENA, 2017, “Renewable Energy: A Key Climate Solution. Tech. Rep. International Renewable Energy Agency (IRENA), 2017, p. 8,” Environ. Prot., pp. 1–8.

[3] “Enerdata. Global Energy Statistical Yearbook 2020. Enerdata, 2020” [Online]. Available: https://yearbook.enerdata.net/total-energy/world-consumption-statistics.html. [Accessed: 25-Apr-2022].

[4] Bilgili, M., Yasar, A., and Simsek, E., 2011, “Offshore Wind Power Development in Europe and Its Comparison with Onshore Counterpart,” Renew. Sustain. Energy Rev., **15**(2), pp. 905–915.

[5] Li, Y., Huang, X., Tee, K. F., Li, Q., and Wu, X. P., 2020, “Comparative Study of Onshore and Offshore Wind Characteristics and Wind Energy Potentials: A Case Study for Southeast Coastal Region of China,” Sustain. Energy Technol. Assessments, **39**, p. 100711.

[6] Enevoldsen, P., and Valentine, S. V., 2016, “Do Onshore and Offshore Wind Farm Development Patterns Differ?,” Energy Sustain. Dev., **35**, pp. 41–51.

[7] Malekjafarian, A., Jalilvand, S., Doherty, P., and Igoe, D., 2021, “Foundation Damping for Monopile Supported Offshore Wind Turbines: A Review,” Mar. Struct., **77**, p. 102937.

[8] Markard, J., and Petersen, R., 2009, “The Offshore Trend: Structural Changes in the Wind Power Sector,” Energy Policy, **37**(9), pp. 3545–3556.

[9] Esteban, M. D., Diez, J. J., López, J. S., and Negro, V., 2011, “Why Offshore Wind Energy?,” Renew. Energy, **36**(2), pp. 444–450.

[10] Ros., J. R. and M. C., 2015, “Floating Offshore Wind: Market and Technology Review Tech. Rep. UK: The Carbon Trust,” p. 167.

[11] “The Leading Edge: April 2020 Wind Energy Newsletter | Wind Research | NREL” [Online]. Available: https://www.nrel.gov/wind/newsletter-202004.html. [Accessed: 16-May-2022].

[12] 2021, “Statistical Review of World Energy Globally Consistent Data on World Energy Markets . and Authoritative Publications in the Field of Energy.”

[13] “London Metal Exchange Database, Steel Billet” [Online]. Available: https://www.lme.com/en/metals/ferrous/lme-steel-rebar-fob-turkey-platts#Trading+day+summary. [Accessed: 16-May-2022].

[14] “INSEE “Indice de Prix de Production de l’industrie Française Pour Le Marché Français - Prix de Base - CPF 23.51 - Ciment - Base 2022” [Online]. Available: https://www.insee.fr/fr/statistiques/serie/010534248. [Accessed: 16-May-2022].

[15] Choisnet, T., 2019, “Initial Comparison of Concrete and Steel Hulls in the Case of IDEOL’S Square Ring Floating Substructure,” (November 2016).

[16] Jiang, D., Tan, K. H., Wang, C. M., Ong, K. C. G., Bra, H., Jin, J., and Kim, M. O., 2018, “Analysis and Design of Floating Prestressed Concrete Structures in Shallow Waters,” Mar. Struct., **59**(February), pp. 301–320.

[17] Wang, C. M., and Tay, Z. Y., 2011, “Very Large Floating Structures: Applications, Research and Development,” Procedia Eng., **14**, pp. 62–72.

[18] Wang, C. M., and Wang, B. T., 2015, *Large Floating Structures Technological Advances*.

[19] Borisade, F., Choisnet, T., and Cheng, P. W., 2016, “Design Study and Full Scale MBS-CFD Simulation of the IDEOL Floating Offshore Wind Turbine Foundation,” J. Phys. Conf. Ser., **753**(9).

[20] Price, S. J., and Figueira, R. B., 2017, “Corrosion Protection Systems and Fatigue Corrosion in Offshore Wind Structures: Current Status and Future Perspectives,” Coatings, **7**(2), pp. 1–51.

[21] Engineering, C., 2019, “Upscaling and Levelized Cost of Energy for Offshore Wind Turbines Supported by Semi-Submersible Floating Platforms,” (January).

[22] Wu, J., and Kim, M., 2021, "Generic Upscaling Methodology of a Floating Offshore Wind Turbine," pp. 1–14.
[23] Stoddard, W., 2002, "The Life and Work of Bill Heronemus, Wind Engineering Pioneer," Wind Eng., **26**(5), pp. 335–341.
[24] Nielsen, F. G., Hanson, T. D., and Skaare, B., 2006, "Integrated Dynamic Analysis of Floating Offshore Wind Turbines," Eur. Wind Energy Conf. Exhib. 2006, EWEC 2006, **3**, pp. 1834–1842.
[25] Fulton, G., Malcolm, D., and Elwany, H., 2007, "Semi-Submersible Platform and Anchor Foundation Systems for Wind Turbine Support," Concept Mar. …, (December).
[26] Roddier, D., Cermelli, C., Aubault, A., and Weinstein, A., 2010, "WindFloat: A Floating Foundation for Offshore Wind Turbines," J. Renew. Sustain. Energy, **2**(3), p. 033104.
[27] Roddier, D., Cermelli, C., and Weinstein, A., 2009, "WindFloat: A Floating Foundation for Offshore Wind Turbines Part I: Design Basis And Qualification Process," pp. 1–9.
[28] Cermelli, C., 2009, "WindFloat: A Floating Foundation for Offshore Wind Turbines Part II: Hydrodynamics Analysis," Engineering, (1), pp. 1–9.
[29] Aubault, A., Cermelli, C., and Roddier, D., 2009, "WindFloat: A Floating Foundation for Offshore Wind Turbines Part III: Structural Analysis," pp. 1–8.
[30] Karimirad, M., and Michailides, C., 2015, "V-Shaped Semisubmersible Offshore Wind Turbine: An Alternative Concept for Offshore Wind Technology," Renew. Energy, **83**, pp. 126–143.
[31] Li, L., Gao, Y., Yuan, Z., Day, S., and Hu, Z., 2018, "Dynamic Response and Power Production of a Floating Integrated Wind, Wave and Tidal Energy System," Renew. Energy, **116**, pp. 412–422.
[32] "Floating Platform | Offshore Wind Power" [Online]. Available: https://www.ideol-offshore.com/en/floatgen-demonstrator. [Accessed: 26-Oct-2019].
[33] Pegalajar-Jurado, A., Bredmose, H., Borg, M., Straume, J. G., Landbø, T., Andersen, H. S., Yu, W., Müller, K., and Lemmer, F., 2018, "State of the Art Model for the LIFES50+ OO Star Wind Floater Semi 10MW Floating Wind Turbine," J. Phys. Conf. Ser., **1104**(1).
[34] Dagher, H. J., Viselli, A. M., Goupee, A. J., Kimball, R., and Allen, C., 2016, "The VolturnUS 1:8 Floating Wind Turbine," **II**.
[35] Borg, M., and Collu, M., 2015, "Offshore Floating Vertical Axis Wind Turbines, Dynamics Modelling State of the Art. Part III: Hydrodynamics and Coupled Modelling Approaches," Renew. Sustain. Energy Rev., **46**, pp. 296–310.
[36] Martin, H. R., 2009, "Development of a Scale Model Wind Turbine for Testing of Offshore Floating Wind Turbine Systems," Univ. Maine, pp. 1–181.
[37] Farrugia, R., Sant, T., and Micallef, D., 2016, "A Study on the Aerodynamics of a Floating Wind Turbine Rotor," Renew. Energy, **86**, pp. 770–784.
[38] Salehyar, S., and Zhu, Q., 2015, "Aerodynamic Dissipation Effects on the Rotating Blades of Floating Wind Turbines," Renew. Energy, **78**, pp. 119–127.
[39] Larsen, T. J., and Hanson, T. D., 2007, "A Method to Avoid Negative Damped Low Frequent Tower Vibrations for a Floating, Pitch Controlled Wind Turbine," *Journal of Physics: Conference Series*, Institute of Physics Publishing.
[40] Odgaard, P. F., Larsen, L. F. S., Wisniewski, R., and Hovgaard, T. G., 2016, "On Using Pareto Optimality to Tune a Linear Model Predictive Controller for Wind Turbines," Renew. Energy, **87**, pp. 884–891.
[41] Jonkman, J. M., 2007, "Dynamics Modeling and Loads Analysis of an Offshore Floating Wind Turbine."
[42] Pegalajar-Jurado, A., Borg, M., and Bredmose, H., 2018, "An Efficient Frequency-Domain Model for Quick Load Analysis of Floating Offshore Wind Turbines," Wind Energy Sci., **3**(2), pp. 693–712.
[43] Suresh, S., 1998, "Fatigue of Materials," Fatigue Mater.
[44] Zenner, H., and Hinkelmann, K., 2019, "August Wöhler – Founder of Fatigue Strength Research," Steel Constr., **12**(2), pp. 156–162.
[45] "Palmgren, A.G. (1924) Die Lebensdauer von Kugellagern (Life Length of Roller Bearings or Durability of Ball Bearings). Zeitschrift Des Vereines Deutscher Ingenieure

(ZVDI), 14, 339-341. - References - Scientific Research Publishing" [Online]. Available: https://www.scirp.org/(S(351jmbntvnsjt1aadkposzje))/reference/ReferencesPapers.aspx?ReferenceID=1754153. [Accessed: 18-May-2022].
[46] Mallet, G. P. (Geoff P., and Transport and Road Research Laboratory., 1991, *Fatigue of Reinforced Concrete.*, H.M.S.O.
[47] Hsu, T. T. C., 1981, "Fatigue of Plain Concrete.," J. Am. Concr. Inst., **78**(4), pp. 292–305.
[48] Khatri, D., 2016, "Structural AnalySiS Discussing Problems, Solutions, and Analysis Methods Fatigue Analysis of Concrete Structures."
[49] 2010, "Fib Bulletin No. 56. Model Code 2010 - First Complete Draft," **2**, pp. 1–288.
[50] 2004, "EN 1992-1-1: Eurocode 2: Design of Concrete Structures - Part 1-1: General Rules and Rules for Buildings."
[51] DNVGL-ST-C502, 2018, "Offshore Concrete Structures," Standard, (February), p. 279.
[52] Islam, M. R., Guo, Y., and Zhu, J., 2014, "A Review of Offshore Wind Turbine Nacelle: Technical Challenges, and Research and Developmental Trends," Renew. Sustain. Energy Rev., **33**, pp. 161–176.
[53] Hoghooghi, H., Chokani, N., and Abhari, R. S., 2021, "A Novel Optimised Nacelle to Alleviate Wind Turbine Unsteady Loads," J. Wind Eng. Ind. Aerodyn., **219**, p. 104817.
[54] REISCH, S., JACOBS, G., BOSSE, D., and MATZKE, D., 2017, "Challenges And Opportunities of Full-Size Nacelle Testing of Wind Turbine Generators," Proc. JSME Int. Conf. motion power Transm., **2017**(0), pp. 10–01.
[55] Lackner, M. A., and Rotea, M. A., 2011, "Passive Structural Control of Offshore Wind Turbines," Wind Energy, **14**(3), pp. 373–388.
[56] Abraham, A., Dasari, T., and Hong, J., 2019, "Effect of Turbine Nacelle and Tower on the near Wake of a Utility-Scale Wind Turbine," J. Wind Eng. Ind. Aerodyn., **193**, p. 103981.
[57] Cox, K., and Echtermeyer, A., 2012, "Structural Design and Analysis of a 10MW Wind Turbine Blade," Energy Procedia, **24**, pp. 194–201.
[58] Bak, Christian; Zahle, Frederik; Bitsche, Robert; Kim, Taeseong; Yde, Anders; Henriksen, Lars Christian; Hansen, Morten Hartvig; Blasques, José Pedro Albergaria Amaral; Gaunaa, Mac; Natarajan, A., 2013, *The DTU 10-MW Reference Wind Turbine*.
[59] Zahle, F., Tibaldi, C., Verelst, D. R., Bak, C., Bitche, R., and Blasquesk, J. P. A. A., 2015, "Aero-Elastic Optimization of a 10 Mw Wind Turbine," 33rd Wind Energy Symp.
[60] Laura Cozzi, B. W., 2019, "Offshore Wind Outlook 2019: World Energy Outlook Special Report. Tech. Rep. International Energy Agency (IEA), 2019, p. 98."
[61] Guillaume, B., Christian, B., Christine, B., Cecile, M., Timothee, P., and Yann, P., 2019, "Design and Performance of a TLP Type Floating Support Structure for a 6MW Offshore Wind Turbine," Proc. Annu. Offshore Technol. Conf., **2019-May**.
[62] Skaare, B., Nielsen, F. G., Hanson, T. D., Yttervik, R., Havmøller, O., and Rekdal, A., 2015, "Analysis of Measurements and Simulations from the Hywind Demo Floating Wind Turbine," (April 2014), pp. 1105–1122.
[63] D, R., C, C., A, A., and A, W., 2010, "WindFloat: A Floating Foundation for Offshore Wind Turbines," J. Renew. Sustain. Energy, **2**, p. 033104.
[64] Chapalain, T., "Semi-Submersible Float, in Particular for an Offshore Wind Turbine."
[65] Mohazzabi, P., 2017, "Archimedes' Principle Revisited," J. Appl. Math. Phys., **5**, pp. 836–843.
[66] Hadžić, I., Hennig, J., Perić, M., and Xing-Kaeding, Y., 2005, "Computation of Flow-Induced Motion of Floating Bodies," Appl. Math. Model., **29**(12), pp. 1196–1210.
[67] Maekawa, K., Ishida, T. and Kishi, T., 2009, *Multi-Scale Modeling of Structural Concrete*, Taylor & Francis.
[68] Maekawa, K., Gebreyouhannes, E., Mishima, T., and An, X., 2006, "Three-Dimensional Fatigue Simulation of RC Slabs under Traveling Wheel-Type Loads," J. Adv. Concr. Technol., **4**(3), pp. 445–457.
[69] Choisnet, T., Rogier, E., Percher, Y., Courbois, A., Crom, I. L. E., and Mariani, R., 2018, "Performance and Mooring Qualification in Floatgen: The First French Offshore Wind Turbine Project," 16ième Journées de l'Hydrodynamique, (June 2018).

[70] "JIS G3101 SS400 Steel Equivalent Material Properties Specification Composition Density Strength" [Online]. Available: https://www.theworldmaterial.com/jis-g3101-ss400-steel-equivalent-material/. [Accessed: 05-Apr-2021].
[71] Japan Concrete Institute, 2007, "STANDARD SPECIFICATIONS FOR CONCRETE STRUCTURES 2007-Design; Japan Society of Civil Engineers," JSCE Guidel. Crack Control.
[72] ACI, A. C. I., 2014, *Building Code Requirements for Structural Concrete*.
[73] ACI Committee 318, 2014, *Aci 318-14*.
[74] ACI, 2007, "Causes , Evaluation , and Repair of Cracks in Concrete Structures as Reported by ACI Committee 224."
[75] Choisnet, T., Favré, M., Lyubimova, M., and Rogier, E., 2014, "A Robust Concrete Floating Wind Turbine Foundation for Worldwide Applications," (July 2014).
[76] Bortolotti, P., Canet Tarres, H., Dykes, K., Merz, K., Sethuraman, L., Verelst, D., and Zahle, F., 2019, *IEA Wind TCP Task 37 Systems Engineering in Wind Energy-WP2.1 Reference Wind Turbines Technical Report*.
[77] Stansberg, C. T. ., Contento, G. ., Seok, W. H. ., Irani, M. ., Ishida, S. ., Mercier, M. ., Wang, Y. ., Wolfram, J. ., Chaplin, J. ., and David, K., " The Specialist Committee on Waves Final Report and Recommendations to the 23rd ITTC. ," Proc. 23rd ITTC, Venice, Italy, 8–14 Sept. 2002; Vol. 2, pp. 505–736.
[78] Suzuki, H.; Shiohara, H.; Schnepf, A.; Houtani, H.; Carmo, L.H.S.; Hirabayashi, S.; Haneda, K.; Chujo, T.; Nihei, Y.; Malta, E.B.; Gonçalves, R. T., 2020, "Wave and Wind Responses of a Very-Light Fowt with Guy-Wired-Supported Tower: Numerical and Experimental Studies," J. Mar. Sci. Eng., **8**(11), pp. 1–21.
[79] Lee, C.-H., 2019, "WAMIT® Manual Version 7.3; WAMIT, Inc.: Chestnut Hill, MA, USA," pp. 1–19.
[80] Jonkman, J. M., Wright, A. D., Hayman, G. J., and Robertson, A. N., 2018, "Full-System Linearization for Floating Offshore Wind Turbines in OpenFAST," ASME 2018 1st Int. Offshore Wind Tech. Conf. IOWTC 2018, pp. 1–10.
[81] DNV, 2021, "DNV-OS-C301 Stability and Water Integrity. DNV, Aug 2021," (August).
[82] "Technomar, 'EdtoolsX User's Manual 2020,' São Paulo, Brazil, [Online] Https://Www.Technomar.Com.Br/ " [Online]. Available: https://www.technomar.com.br/. [Accessed: 21-Feb-2022].
[83] FALTINSEN, O. M., 1993, *Sea Loads on Ships and Offshore Structures | TU Delft Repositories*.
[84] Takata, T., Takaoka, M., Gonçalves, R. T., Houtani, H., Yoshimura, Y., Hara, K., Oh, S., Iijima, K., and Suzuki, H., 2021, "Dynamic Behavior of a Flexible Multi-Column FOWT in Regular Waves," J. Mar. Sci. Eng., **9**(124).
[85] Jonkman, J.M.; Buhl, M.L., J., 2005, "FAST User's Guide Updated August 2005; Technical Report; NREL/TP-500-38230," Natl. Renew. Energy Lab. [Online]. Available: https://www.nrel.gov/wind/nwtc/ openfast.html.
[86] OTANI, M., 2006, "PC / Steel Composite Cable-Stayed Bridge Using Corrugated Steel Web - Outline of TOYOTA-Arrows-Bridge," **25**, pp. 36–41.